

# Spectral Solar Irradiance and Its Entropic Effect on Earth's Climate

Wei Wu<sup>1</sup>, Yangang Liu<sup>1</sup>, and Guoyong Wen<sup>2,3</sup>

<sup>1</sup>Atmospheric Sciences Division, Brookhaven National Laboratory, Upton, NY 11973, USA

<sup>2</sup>NASA Goddard Space Flight Center, Greenbelt, Maryland, USA

<sup>3</sup>Goddard Earth Sciences and Technology Center, University of Maryland, Baltimore, Maryland, USA

Submission for publication in *Earth System Dynamics*

(*Special Issue on Thermodynamics of the Earth System*)

(A revision, submitted on March 05, 2011)

Corresponding author:

Wei Wu

Atmospheric Sciences Division

Brookhaven National Laboratory

75 Rutherford Dr., Bldg. 815E

Upton, NY 11973

Email: [wwu@bnl.gov](mailto:wwu@bnl.gov)

## Abstract

The high-resolution measurements of the spectral solar irradiance at the top of the Earth's atmosphere by the Solar Radiation and Climate Experiment (SORCE) satellite are used to examine the magnitude and spectral distribution of the Earth's incident solar radiation entropy flux. The Earth's incident solar radiation entropy flux estimated by directly applying the observed spectral solar irradiance into the most accurate Planck expression under two different assumptions is examined and further compared with that estimated with a conventional approach that uses the Sun's brightness temperature under the assumption of a blackbody Sun. The globally averaged non-blackbody incident solar radiation entropy flux at the top of the Earth's atmosphere equals  $0.31 \text{ W m}^{-2} \text{ K}^{-1}$  under the assumption I of isotropic hemispheric solar radiation, or  $0.08 \text{ W m}^{-2} \text{ K}^{-1}$  under the assumption II that the specific solar energy intensity received at the TOA is the same as that radiated at the Sun's surface and incident solar radiation is isotropic within the cone of the solid angle to the Sun subtended by any point at the TOA. The former is about 4 times larger than that estimated from the conventional blackbody approach, with the difference comparable to the typical value of the entropy production rate associated with atmospheric latent heat process. The latter is about the same as that estimated from the conventional blackbody approach. Sensitivity study further shows that the distribution of top-of-atmosphere spectral solar irradiance could significantly impact the magnitude and spectral distribution of the estimated Earth's incident solar radiation entropy flux. These results together suggest that the spectral distribution of incident solar radiation is critical for determining the Earth's incident solar radiation entropy flux, and thus the Earth's climate.

## **1. Introduction**

Modern satellite observations have demonstrated that although the total solar irradiance (TSI) at the top of the Earth's atmosphere (TOA) varies little (only about 0.1%), the Sun is a highly variable star with a substantial variation of TOA spectral solar irradiance (SSI) (Harder et al., 2010). Because solar radiation is the primary driving force for all the activities within the Earth's climate system and radiation at different wavelengths reaches and warms different atmospheric layers, this finding raises some important questions critical to studying the Earth's climate system: What is the consequence of the changing TOA SSI to the Earth's climate system? Could this finding change our view of greenhouse-gas induced global climate change?

Based on the daily observations of the solar spectrum between 200 nm and 2400 nm from the Spectral Irradiance Monitor (SIM) instrument on the Solar Radiation and Climate Experiment (SORCE) satellite, Harder et al. (2010) found that the primary contributors to TSI (i.e., irradiance at ultraviolet, visible, and near infrared wavelengths) exhibit significantly different variability with time. The irradiance at ultraviolet (200 nm to 400 nm) wavelengths shows a significant decline from 04/2004 to 02/2008 while the irradiance at visible (400 nm to 691 nm) or near infrared (972 nm to 2423 nm) wavelengths shows a large increase and the irradiance at near infrared (691 nm to 972 nm) wavelengths shows a small decrease (see Figure 3 in Harder et al., 2010). It has been known that radiation at ultraviolet wavelengths mainly heats stratosphere and is critical to producing stratospheric ozone, and radiation at visible and near infrared wavelengths mainly heats troposphere as well as the Earth's surface. Thus, the significantly different variability of the primary contributors to TSI is intuitively expected to

have a large impact on the vertical profiles of atmospheric ozone and temperature as well as the Earth's surface temperature.

A series of recent papers has investigated the Earth's climate responses to the TOA SSI variability as reported by Harder et al. (2010), suggesting that the impacts of the TOA SSI variability on the Earth's climate system could be significantly different from our current understanding, especially on the vertical profiles of atmospheric ozone and temperature (e.g., Cahanlan et al. 2010; Haigh et al., 2010). For example, Cahanlan et al. (2010) used the findings by Harder et al. (2010) to construct two 11-year sinusoidal scenarios of TOA SSI forcing with the same TSI. One has out-of-phase SSI variability as in the SIM-based observations and the other has in-phase SSI variability as the reconstructed solar radiation from a widely used solar radiation reconstruction model by Lean (2000). Then, they used the two scenarios of TOA SSI forcing to drive a radiative-convective model and a global climate model (i.e., NASA Goddard Institute for Space Studies modelE) to investigate the difference of the Earth's climate responses. They found that the two scenarios lead to significantly different climate responses, especially in upper stratosphere where temperature response to the out-of-phase scenario shows 5 times larger than that to the in-phase scenario. Additionally, Haigh et al. (2010) employed a radiative photochemical model to investigate the impact of the SIM-based out-of-phase TOA SSI variability on stratosphere by comparing with the Lean-model reconstructed in-phase TOA SSI variability. They found that the SIM-based out-of-phase TOA SSI variability could lead to a significant decline in stratospheric ozone below an altitude of 45 km from 2004 to 2007 and an increase above this altitude. Besides, they also found that according to the SIM-based TOA SSI observations the tropopause SSI has an increase over the declining phase of solar cycle 23 (i.e., out-of-phase with declining solar activity from 2004 to 2007), which is opposite to our previous

understanding. Furthermore, Gray et al. (2010) reviewed current understanding of the influence of solar variability on the Earth's climate system from solar variability, solar-terrestrial interactions and the mechanisms determining the response of the Earth's climate system. They emphasized that if the out-of-phase TOA SSI variability in the SIM-based observations is real, responses in both stratospheric ozone and temperature are expected to be much different from current expectations as indicated by Haigh et al. (2010) and thus need to be reassessed. They suggested a need of further observations and research for improving our understanding of solar forcing mechanisms and their impacts on the Earth's climate system, including understanding the SIM-based out-of-phase TOA SSI variability and assessing their influence on the Earth's climate system.

Here, we are motivated to investigate entropic impact of the SIM-based out-of-phase TOA SSI variability on the Earth's climate system. Entropy, as a fundamental thermodynamic quantity additional to temperature and energy, has been shown critical for studying the Earth's climate system (e.g., Pujol and Fort, 2002; Ozawa et al., 2001; Paltridge et al., 2007; Pauluis et al. 2002a, 2002b; Wang et al., 2008; Lucarini et al. 2010; Jupp and Cox, 2010; Lorenz, 2010; Wu and Liu, 2010b; Liu et al., 2011). A broad range of entropy applications on the Earth's biosphere-atmosphere system including aspects such as atmospheric circulation, role of clouds, hydrology, ecosystem exchange of energy and mass can be found in a special issue published in *Philosophical Transactions of the Royal Society B* (Kleidon et al., 2010). The radiation exchange between the Earth's climate system and its surrounding space provides us not only the thermodynamic constraint of energy conservation dictated by the first law of thermodynamics but also the thermodynamic constraint of the overall entropy increase of the Earth's climate system associated with the second law of thermodynamics (e.g., Wu and Liu, 2010a). It is

anticipated that integration of this entropy-related thermodynamic constraint into current global climate models will improve our understanding of the Earth's climate and climate change.

A proper approach to accurately calculating the overall entropy increase of the Earth's climate system is the key to investigating the entropic properties of the Earth's climate system. Calculation of the Earth's overall entropy change in turn requires knowledge of radiation entropy from the Earth's incident solar radiation (incident solar radiation entropy hereafter), radiation entropy from the Earth's reflected solar radiation, and radiation entropy from the Earth's emitted terrestrial radiation. The reflected solar and emitted terrestrial radiation entropies and the approaches for estimating them have been studied in previous papers (e.g., Stephens and O'Brien, 1993; Wu and Liu, 2010a). However, the incident solar radiation entropy has rarely been investigated, especially from the perspective of incident spectral solar irradiance.

This paper focuses on examining the entropic impact of the SIM-based out-of-phase TOA SSI variability on the Earth's climate system. Conventionally, the Earth's incident solar radiation entropy is estimated by using the Sun's brightness temperature under the assumption of a blackbody Sun as proposed by Stephens and O'Brien (1993). However, the SIM-based TOA SSI measurements indicate that solar radiation does not follow the blackbody radiation law as commonly assumed. Here, we take advantage of the SIM-based TOA SSI observations to investigate the magnitude and spectral distribution of the Earth's incident solar radiation entropy flux, and to examine the significance of the impact of TOA SSI variability on estimation of the Earth's incident solar radiation entropy flux.

Section 2 briefly introduces data and methodology used in this study. Section 3 shows the spectral distribution of the Earth's incident solar radiation entropy flux estimated by using the SIM-based TOA SSI observations under two different assumptions of incident solar radiation.

The estimated Earth's incident solar radiation entropy flux from the SIM-based TOA SSI observations is further compared with a conventional estimate by using the Sun's brightness temperature under the assumption of a blackbody Sun. Section 4 investigates the potential cause of the difference among the estimates, by analyzing specific solar entropy intensity and solar entropy flux at the TOA. Section 5 examines the sensitivity of the Earth's incident solar radiation entropy flux to TOA SSI variability. Section 6 summarizes the main results.

## 2. Data and Methodology

Daily observations of TOA SSI between 200 nm and 2400 nm have been produced through the SIM instrument on SORCE satellite since February 2003. Discussions on the SORCE SIM instrument and its product of TOA SSI data can be found in Harder et al. (2005) and Rottman et al. (2005). We use the daily SIM-based TOA SSI observations from 04/2004 to 10/2010 for this study of investigating the magnitude and spectral distribution of the Earth's incident solar radiation entropy flux. The corresponding daily TOA TSI observations from the Total Irradiance Monitor (TIM) instrument on SORCE satellite are also used as a constraint of the overall solar irradiance reaching the Earth's climate system.

It is well established that Planck expression given by Eq. (1) or Eq. (2) can be used to calculate the spectral radiation entropy flux from the spectral radiation energy flux for any radiation process (Wei and Liu 2010a).

$$L_\nu = \frac{2K\nu^2}{c^2} \left\{ \left( 1 + \frac{c^2 I_\nu}{2h\nu^3} \right) \ln \left( 1 + \frac{c^2 I_\nu}{2h\nu^3} \right) - \left( \frac{c^2 I_\nu}{2h\nu^3} \right) \ln \left( \frac{c^2 I_\nu}{2h\nu^3} \right) \right\} \quad (1)$$

or

$$L_{\lambda} = \frac{2\kappa c}{\lambda^4} \left\{ \left( 1 + \frac{\lambda^5 I_{\lambda}}{2hc^2} \right) \ln \left( 1 + \frac{\lambda^5 I_{\lambda}}{2hc^2} \right) - \left( \frac{\lambda^5 I_{\lambda}}{2hc^2} \right) \ln \left( \frac{\lambda^5 I_{\lambda}}{2hc^2} \right) \right\} \quad (2)$$

where  $I_{\nu}$  (or  $I_{\lambda}$ ) and  $L_{\nu}$  (or  $L_{\lambda}$ ) represent spectral radiation energy and entropy fluxes per unit frequency (or wavelength) per unit solid angle per unit area (hereafter called ‘specific energy intensity’ and ‘specific entropy intensity’) respectively,  $h, c$  and  $\kappa$  are the Planck constant, speed of light in vacuum and the Boltzmann constant respectively, and  $\nu$  (or  $\lambda$ ) represents frequency (or wavelength) variable. Planck expression was originally formulated for calculating specific entropy intensity of a monochromatic (blackbody) radiation beam at thermodynamic equilibrium (Planck, 1913), and has been later demonstrated to hold also for non-blackbody radiation at a non-equilibrium condition (e.g., Wu and Liu, 2010a).

The Earth’s incident solar radiation entropy flux  $J$  can then be obtained by integrating the Earth’s incident specific solar entropy intensity over all the frequencies (or wavelengths) through a surface with a known zenith angle  $\theta$  and solid angle  $\Omega$ ,

$$J = \int_0^{\infty} d\nu \int_{\Omega} L_{\nu} \cos \theta d\Omega \quad (3)$$

or

$$J = \int_0^{\infty} d\lambda \int_{\Omega} L_{\lambda} \cos \theta d\Omega \quad (4)$$

Here, we use Planck expression to estimate the Earth’s incident spectral solar radiation entropy flux from the Earth’s incident specific solar entropy intensity, and the Earth’s incident solar radiation entropy flux derived from (3) or (4) is referred to the exact result. We examine the exact result under two different assumptions: I. isotropic hemispheric solar radiation, i.e., the

geometric factor  $\int \cos \theta d\Omega = \int_0^{2\pi} d\varphi \int_0^{\pi/2} \sin \theta \cos \theta d\theta = \pi$ ; II. the specific solar energy intensity received at the TOA is the same as that radiated at the Sun's surface and incident solar radiation is isotropic within the cone of the solid angle to the Sun subtended by any point at the TOA.

Another approach examined is that presented in Stephens and O'Brien (1993). Assuming that the Sun follows blackbody radiation law, Stephens and O'Brien (1993) developed an approximate expression that relates the Earth's incident solar radiation entropy flux to the Sun's brightness temperature  $T_{Sun}$ ,

$$J = \frac{4}{3} \sigma T_{Sun}^3 \cos \theta_0 \frac{\Omega_0}{\pi} \quad (5)$$

where  $\theta_0$  represents globally averaged solar zenith angle and  $\Omega_0$  represents solar solid angle to the Earth.

The entropic impact of the SIM-based TOA SSI observations on estimation of the Earth's incident solar radiation entropy flux will be investigated by comparing the exact result of the Earth's incident solar radiation entropy flux from using Planck expression and the SIM-based TOA SSI observations under the two different assumptions with the conventional result from using the expression (5) and the Sun's brightness temperature under the assumption of a blackbody Sun, and by testing the sensitivity of the magnitude and spectral distribution of the Earth's incident solar radiation entropy flux to TOA SSI variability.

### **3. The Earth's incident solar radiation entropy flux**

In this section, we first estimate the exact Earth's incident solar radiation entropy flux by using Planck expression and the SIM-based TOA SSI observations. The exact Earth's incident solar

radiation entropy flux is then compared with that estimated by using the conventional expression (5) and the Sun's brightness temperature under the assumption of a blackbody Sun.

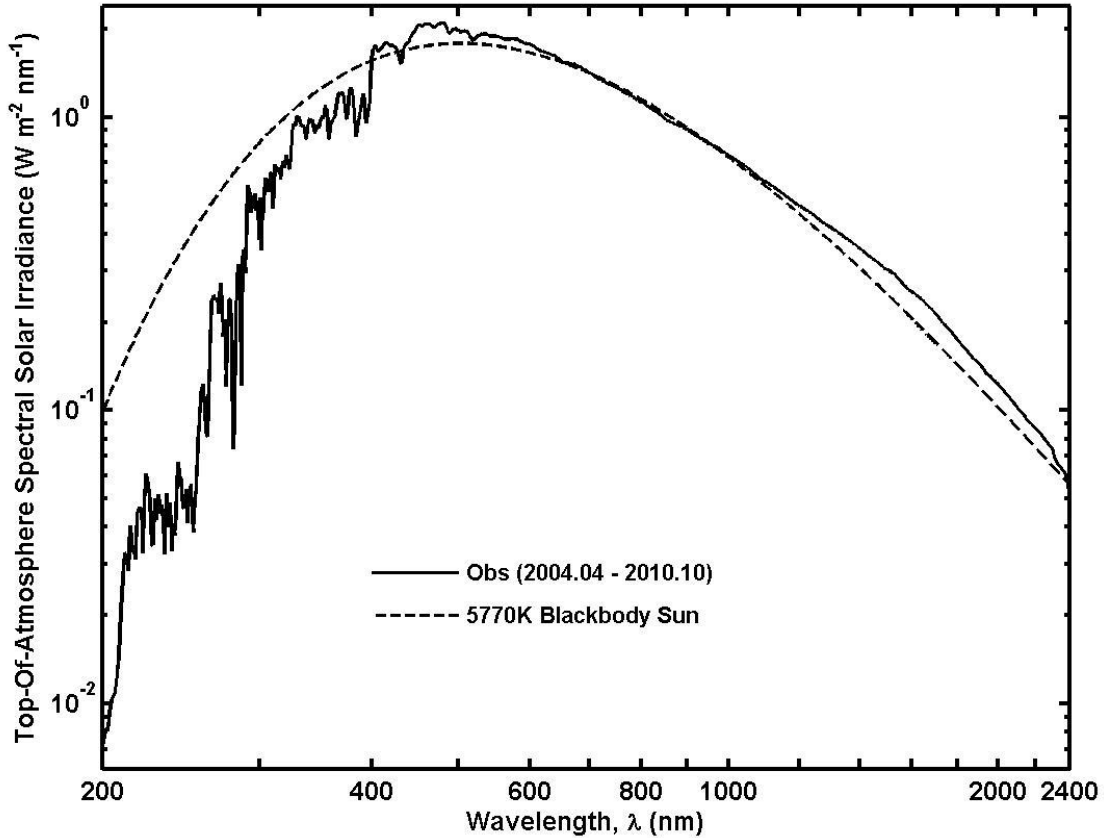


Figure 1. Black solid line represents the mean SIM-based TOA SSI distribution based on the data collected from 04/2004 to 10/2010. Black dashed line represents the TOA SSI distribution corresponding to a blackbody Sun with brightness temperature 5770 K.

Figure 1 shows the mean SIM-based TOA SSI distribution (black solid line) based on the data collected from 04/2004 to 10/2010. As a comparison, the TOA SSI distribution (black

dashed line) corresponding to a blackbody Sun with brightness temperature 5770 K is also shown in Figure 1. The blackbody Sun provides the TOA TSI of  $1361 \text{ W m}^{-2}$  as the mean TIM-based TOA TSI observations from 04/2004 to 10/2010. Similar to the findings in Harder et al. (2010, Figure 2), Figure 1 shows that the irradiance at ultraviolet ( $< 400 \text{ nm}$ ) wavelengths in the SIM-based TOA SSI is much smaller in magnitude than that in the TOA SSI of the blackbody Sun, suggesting that the brightness temperature of solar radiation at ultraviolet wavelengths is much cooler than that of the blackbody Sun. On the contrary, the irradiance over visible (400 nm to 700 nm) or the near-infrared (1000 nm to 2400 nm) wavelengths in the SIM-based TOA SSI is larger than that in the TOA SSI of the blackbody Sun, reflecting that the brightness temperature of solar radiation at visible and the near-infrared wavelengths is hotter than that of the blackbody Sun. The irradiance at the near-infrared (700 nm to 1000 nm) wavelengths in the SIM-based TOA SSI shows slightly relatively cooler than that in the TOA SSI of the blackbody Sun.

TOA specific solar energy intensity ( $I_\lambda$ ) can be estimated using known TOA SSI under the two assumptions: I. isotropic hemispheric solar radiation, II. the specific solar energy intensity received at the TOA is the same as that radiated at the Sun's surface and the incident solar radiation is isotropic within the cone of the solid angle to the Sun subtended by any point at the TOA. Detailed discussions on the difference of the resulting TOA specific solar energy (or entropy) intensity under the two assumptions are provided in the next section.

Substitution of the TOA specific solar energy intensity ( $I_\lambda$ ) corresponding to Figure 1 into Planck expression leads to the estimates of TOA specific solar entropy intensity ( $L_\lambda$ ). Integration of the TOA  $L_\lambda$  over the solid angle of incident solar radiation leads to the

corresponding estimates of the Earth's incident spectral solar radiation entropy flux (shown in Figure 2).

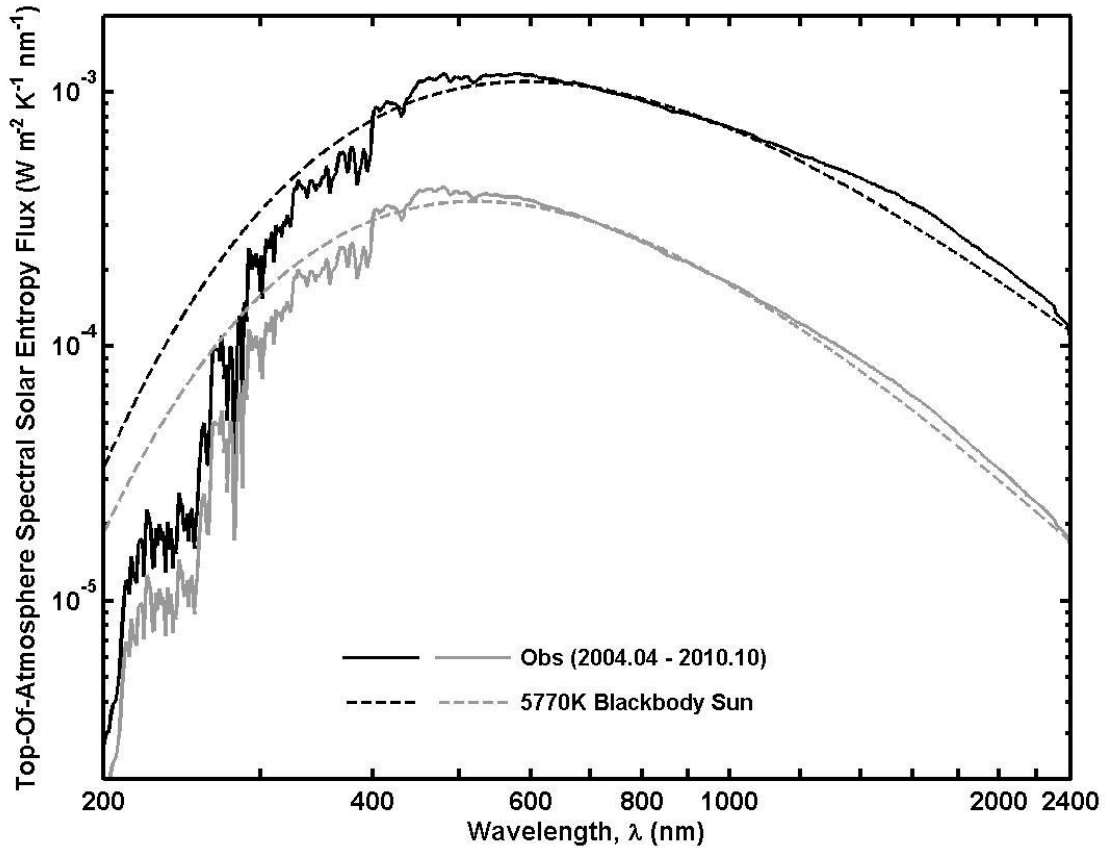


Figure 2. The Earth's incident spectral solar radiation entropy flux corresponding to the TOA SSIs as shown in Figure 1. Black solid and dashed lines are calculated under the assumption I of isotropic hemispheric solar radiation. Gray solid and dashed lines are calculated under the assumption II that the specific solar energy intensity received at the TOA is the same as that radiated at the Sun's surface and incident solar radiation is isotropic within the cone of the solid angle to the Sun subtended by any point at the TOA.

It is noticeable that the patterns of spectral solar radiation entropy flux under the two assumptions look almost identical, except that the magnitude of the spectral solar radiation entropy flux under the assumption I is larger than that under the assumption II. The distinction of the resulting spectral solar radiation entropy flux between the two assumptions increases with wavelength. It is also evident that the estimates of the Earth's incident spectral solar radiation entropy flux exhibit remarkably similar patterns to their corresponding SSI distributions as shown in Figure 1. For example, the Earth's incident solar radiation entropy flux from the SIM-based TOA SSI shows relatively low entropy flux at ultraviolet (< 400 nm) wavelengths, relatively high entropy flux at visible (400 nm to 700 nm) and the near-infrared (1000 nm to 2400 nm) wavelengths, and slightly relatively low entropy flux at the near-infrared (700 nm to 1000 nm) wavelengths. The overall Earth's incident solar radiation entropy flux within [200nm, 2400nm] wavelengths under the assumption I is equal to  $1.13 \text{ W m}^{-2} \text{ K}^{-1}$  for the SIM-based TOA SSI, or  $1.08 \text{ W m}^{-2} \text{ K}^{-1}$  for the blackbody Sun. The overall Earth's incident solar radiation entropy flux within [200nm, 2400nm] wavelengths under the assumption II is equal to  $0.30 \text{ W m}^{-2} \text{ K}^{-1}$  for both the SIM-based TOA SSI and for the blackbody Sun.

If we assume that the TOA SSI outside [200nm, 2400nm] wavelengths corresponding to the SIM-based TOA SSI observations is equal to a constant fraction of the blackbody Sun's TOA SSI at the same wavelengths with its overall TSI of  $1361 \text{ W m}^{-2}$ , we obtain the overall Earth's incident solar radiation entropy flux corresponding to the SIM-based TOA SSI through Planck expression of  $1.24 \text{ W m}^{-2} \text{ K}^{-1}$  under the assumption I, and of  $0.31 \text{ W m}^{-2} \text{ K}^{-1}$  under the assumption II. For the blackbody Sun, the obtained overall Earth's incident solar radiation entropy flux equals  $1.23 \text{ W m}^{-2} \text{ K}^{-1}$  under the assumption I, or equals  $0.31 \text{ W m}^{-2} \text{ K}^{-1}$  under the assumption II. In other words, the difference of the obtained overall Earth's incident solar

radiation entropy fluxes from the SIM-based TOA SSI observations or from the blackbody Sun is small under either of the two assumptions. The globally averaged Earth's incident solar radiation entropy flux (i.e., one quarter of the Earth's incident solar radiation entropy flux over a plane perpendicular to the cone of incident solar beams, see detailed derivation in the next section) equals  $0.31 \text{ W m}^{-2} \text{ K}^{-1}$  for both the SIM-based TOA SSI observations and for the blackbody Sun under the assumption I, and equals  $0.08 \text{ W m}^{-2} \text{ K}^{-1}$  for both the SIM-based TOA SSI observations and for the blackbody Sun under the assumption II. In other words, the globally averaged Earth's incident solar radiation entropy flux under the assumption I is about 4 times larger than that under the assumption II.

On the other hand, using the same blackbody Sun's brightness temperature ( $T_{Sun} = 5770 \text{ K}$ ), and assuming the globally averaged cosine of solar zenith angle  $\cos \theta_0 = 0.25$  and solar solid angle  $\Omega_0 = 6.77 \times 10^{-5} \text{ sr}$  to the planet as in Stephens and O'Brien (1993), the conventional expression (5) yields the Earth's incident solar radiation entropy flux of  $0.08 \text{ W m}^{-2} \text{ K}^{-1}$ , about the same value as that from either the SIM-based TOA SSI observations or the blackbody Sun under the assumption II.

## **4. Specific solar entropy intensity and solar entropy flux at the TOA**

### **4.1. Specific solar entropy intensity**

Relative to the estimated Earth's incident solar radiation entropy flux under the assumption I (i.e., isotropic hemispheric solar radiation), the entropy flux estimated under the assumption II (i.e., the specific solar energy intensity received at the TOA is the same as that radiated at the Sun's surface and incident solar radiation is isotropic within the cone of the solid angle to the

Sun subtended by any point at the TOA) or estimated from the conventional approach exhibits significantly lower value. Further inspection reveals that the large difference can be attributed to the fact that the specific solar entropy intensity at the TOA defined under the two different assumptions has different physical meaning. Also, the conventional approach is demonstrated to match the formula of the globally averaged Earth's incident solar radiation entropy flux under the assumption II for a blackbody Sun. This section explores this issue.

Suppose that the Sun is a blackbody with brightness temperature of  $T_{Sun}$ , the specific solar energy ( $I_{\lambda}^{Sun}$ ) and entropy ( $L_{\lambda}^{Sun}$ ) intensities at the Sun's surface can be written as (based on Planck's radiation theory by Planck, 1913)

$$I_{\lambda}^{Sun} = \frac{2hc^2}{\lambda^5} \left\{ \frac{1}{\exp\left(\frac{hc}{\lambda kT_{Sun}}\right) - 1} \right\} \quad (6)$$

$$L_{\lambda}^{Sun} = \frac{2\kappa c}{\lambda^4} \left\{ \left(1 + \frac{\lambda^5 I_{\lambda}^{Sun}}{2hc^2}\right) \ln\left(1 + \frac{\lambda^5 I_{\lambda}^{Sun}}{2hc^2}\right) - \left(\frac{\lambda^5 I_{\lambda}^{Sun}}{2hc^2}\right) \ln\left(\frac{\lambda^5 I_{\lambda}^{Sun}}{2hc^2}\right) \right\} \quad (7)$$

When the solar radiation travels in space to a point with a distance  $r$  (e.g., 1 AU) to the Sun, the specific solar entropy intensity at this point ( $I_{\lambda}^r$ ) depends on the nature of how the solar radiation is received. Below are the detailed results under the two typical assumptions.

#### 4.1.1. Assumption I

Assumption I assumes an isotropic hemispheric solar radiation at the TOA. Under this assumption, the specific solar energy intensity at this place ( $I_\lambda^r$ ) is inversely proportional to the square of the distance  $r$ , i.e.,

$$I_\lambda^r = \frac{r_{Sun}^2}{r^2} I_\lambda^{Sun} \quad (8)$$

or

$$\frac{I_\lambda^r}{I_\lambda^{Sun}} = \frac{r_{Sun}^2}{r^2} \quad (9)$$

where  $r_{Sun}$  represents the Sun's radius. Equation (9) indicates that the ratio of  $\frac{I_\lambda^r}{I_\lambda^{Sun}}$  is a wavelength independent variable, varying only with the distance  $r$ .

Substitution of the specific solar energy intensity  $I_\lambda^r$  into Planck expression (2), we obtain the corresponding specific solar entropy intensity at this place ( $L_\lambda^r$ ) as

$$\begin{aligned} L_\lambda^r &= \frac{2\kappa C}{\lambda^4} \left\{ \left( 1 + \frac{\lambda^5 I_\lambda^r}{2hc^2} \right) \ln \left( 1 + \frac{\lambda^5 I_\lambda^r}{2hc^2} \right) - \left( \frac{\lambda^5 I_\lambda^r}{2hc^2} \right) \ln \left( \frac{\lambda^5 I_\lambda^r}{2hc^2} \right) \right\} \\ &= \frac{2\kappa C}{\lambda^4} \left\{ \left( 1 + \frac{r_{Sun}^2}{r^2} \frac{\lambda^5 I_\lambda^{Sun}}{2hc^2} \right) \ln \left( 1 + \frac{r_{Sun}^2}{r^2} \frac{\lambda^5 I_\lambda^{Sun}}{2hc^2} \right) - \left( \frac{r_{Sun}^2}{r^2} \frac{\lambda^5 I_\lambda^{Sun}}{2hc^2} \right) \ln \left( \frac{r_{Sun}^2}{r^2} \frac{\lambda^5 I_\lambda^{Sun}}{2hc^2} \right) \right\} \end{aligned} \quad (10)$$

Based on Eqs. (7) and (10), we obtain

$$\frac{L_\lambda^r}{L_\lambda^{Sun}} = \frac{\left( 1 + \frac{r_{Sun}^2}{r^2} \frac{\lambda^5 I_\lambda^{Sun}}{2hc^2} \right) \ln \left( 1 + \frac{r_{Sun}^2}{r^2} \frac{\lambda^5 I_\lambda^{Sun}}{2hc^2} \right) - \left( \frac{r_{Sun}^2}{r^2} \frac{\lambda^5 I_\lambda^{Sun}}{2hc^2} \right) \ln \left( \frac{r_{Sun}^2}{r^2} \frac{\lambda^5 I_\lambda^{Sun}}{2hc^2} \right)}{\left( 1 + \frac{\lambda^5 I_\lambda^{Sun}}{2hc^2} \right) \ln \left( 1 + \frac{\lambda^5 I_\lambda^{Sun}}{2hc^2} \right) - \left( \frac{\lambda^5 I_\lambda^{Sun}}{2hc^2} \right) \ln \left( \frac{\lambda^5 I_\lambda^{Sun}}{2hc^2} \right)} \quad (11)$$

Equation (11) indicates that unlike the wavelength-independent ratio of the specific solar energy intensity at a place  $r$  ( $I_{\lambda}^r$ ) and that at the Sun's surface ( $I_{\lambda}^{Sun}$ ) [see Eq. (9)], the ratio of the specific solar entropy intensity at a place  $r$  ( $L_{\lambda}^r$ ) and that at the Sun's surface ( $L_{\lambda}^{Sun}$ ) varies with both wavelength  $\lambda$  and the distance  $r$ .

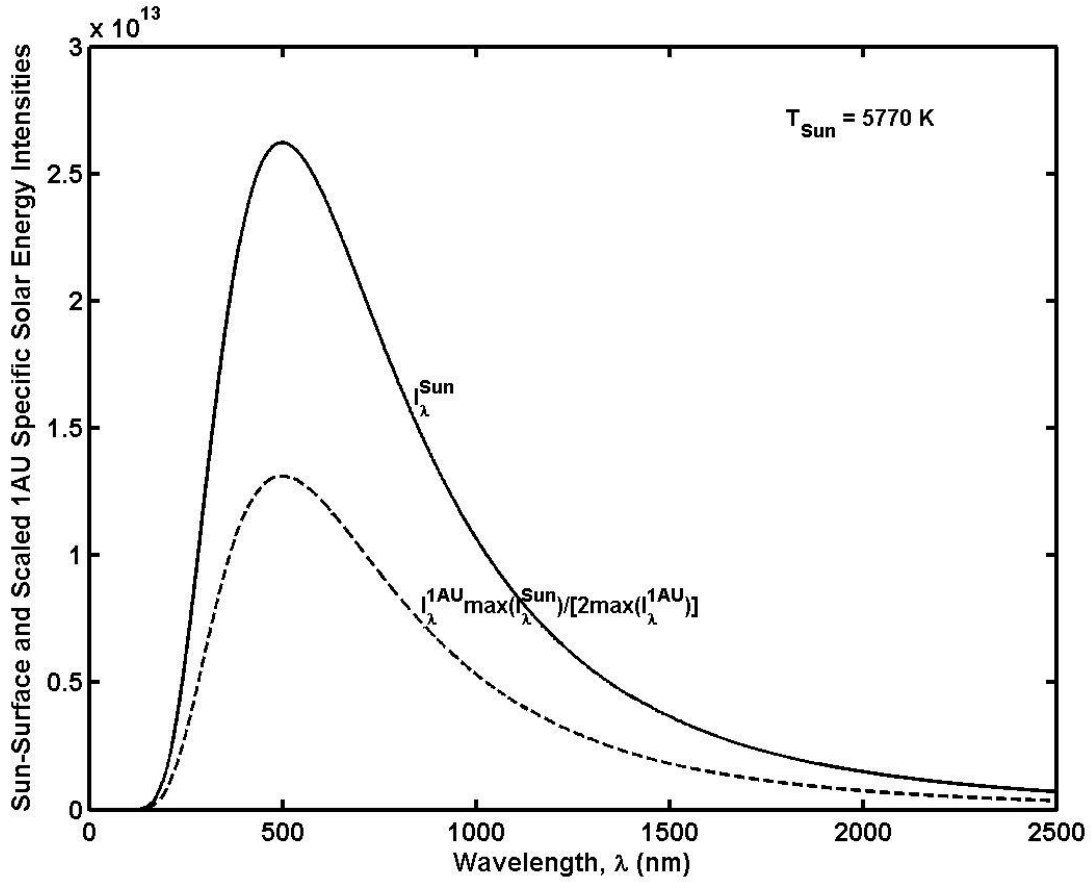


Figure 3. Specific solar energy intensity at the Sun's surface (black solid line) and that at 1 AU scaled by  $\{\max(I_{\lambda}^{Sun})/[2\max(I_{\lambda}^{1AU})]\}$  (black dashed line), for a blackbody Sun with brightness temperature 5770 K under the assumption I of isotropic hemispheric solar radiation.

Figure 3 shows the specific solar energy intensity at the Sun's surface (black solid line) and that at 1 AU scaled by  $\{\max(I_{\lambda}^{Sun})/[2\max(I_{\lambda}^{1AU})]\}$  (black dashed line), for a blackbody Sun with brightness temperature 5770 K under the assumption I. Here, we use the Sun's radius of  $6.96 \times 10^8$  m and the 1AU distance to the Sun of  $1.49598 \times 10^{11}$  m. As expected, the two curves exhibit the same spectral distributions with one's amplitude being a constant fraction of the others. Both peak at the same wavelength. In fact, the 1AU specific solar energy intensity is not a representative of a blackbody's specific solar energy intensity as discussed in previous papers (e.g., Figure 2 in Wu and Liu, 2010a).

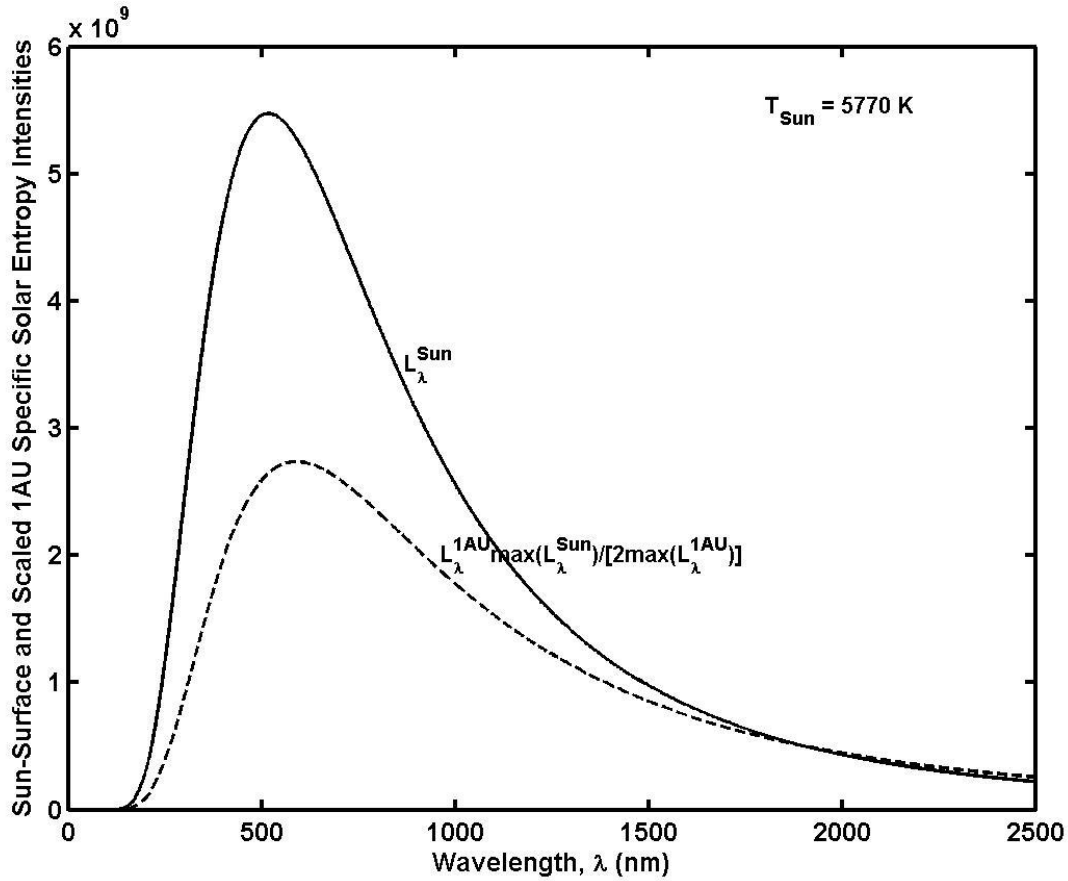


Figure 4. Specific solar entropy intensity at the Sun’s surface (black solid line) and that at 1 AU scaled by  $\{\max(L_{\lambda}^{Sun})/[2\max(L_{\lambda}^{1AU})]\}$  (black dashed line), for a blackbody Sun with brightness temperature 5770 K under the assumption I of isotropic hemispheric solar radiation.

Figure 4 shows the specific solar entropy intensity at the Sun’s surface (black solid line) and that at 1 AU scaled by  $\{\max(L_{\lambda}^{Sun})/[2\max(L_{\lambda}^{1AU})]\}$  (black dashed line), for the blackbody Sun with brightness temperature 5770 K under the assumption I as in Figure 3. Unlike the specific solar energy intensities at the Sun’s surface and that at 1 AU which have the same spectral distributions, the spectral distributions of the two corresponding specific solar entropy

intensities are different. As can be seen from Figure 4, the peak of the specific solar entropy intensity at 1 AU slightly shifts to the right (larger wavelength) compared with that at the Sun's surface. In addition, the reduction on amplitude of the specific solar entropy intensity because of radiation traveling distance shown in Figure 4 is wavelength dependent.

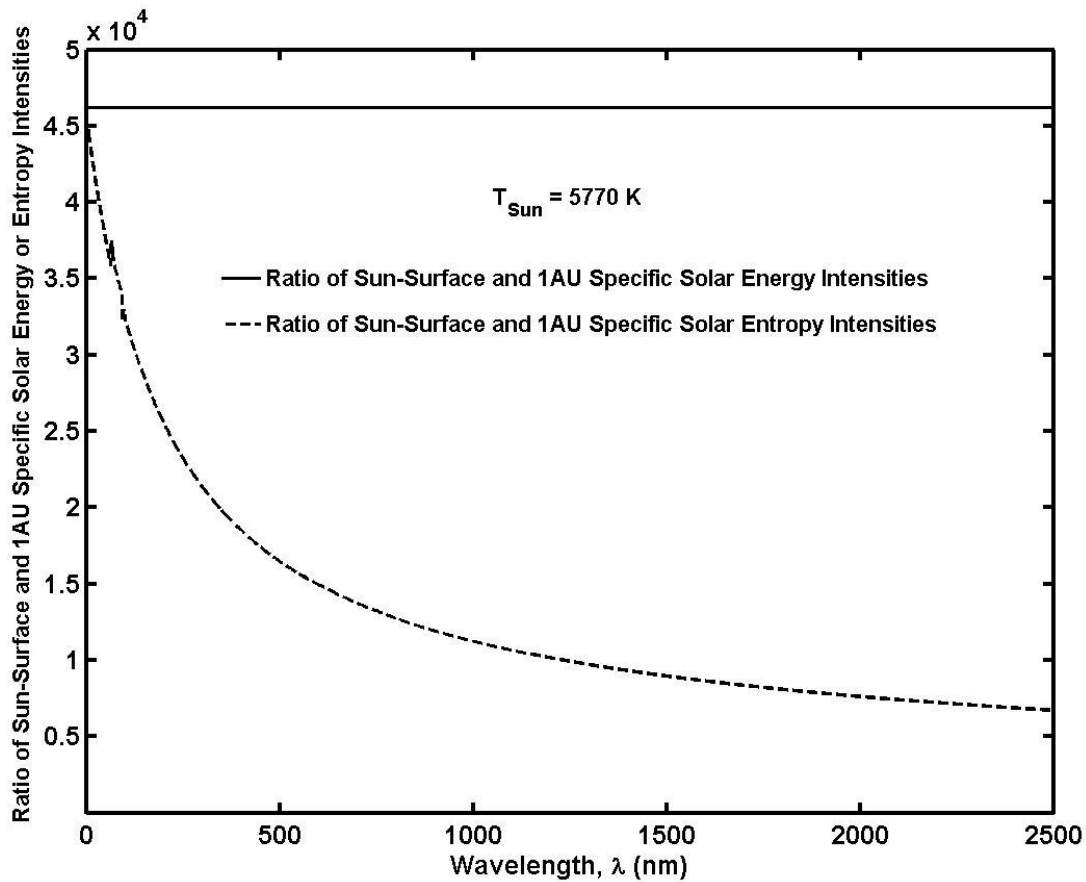


Figure 5. Black solid line: the ratio of specific solar energy intensity at the Sun's surface and that at 1 AU, for a blackbody Sun with brightness temperature 5770 K under the assumption I of isotropic hemispheric solar radiation. Black dashed line: the ratio of specific solar entropy intensity at the Sun's surface and that at 1 AU for the same blackbody Sun under the assumption I of isotropic hemispheric solar radiation.

Figure 5 further illustrates this point by plotting the ratio of specific solar energy intensity at the Sun's surface and that at 1 AU (i.e.,  $I_{\lambda}^{Sun} / I_{\lambda}^{1AU}$ ) and the ratio of specific solar entropy intensity at the Sun's surface and that at 1 AU (i.e.,  $L_{\lambda}^{Sun} / L_{\lambda}^{1AU}$ ). The former presents a constant for all the wavelengths but the latter decreases quickly with the increase of wavelength.

#### 4.1. 2 Assumption II

Assumption II assumes that the specific solar energy intensity received at the TOA is the same as that radiated at the Sun's surface and incident solar radiation is isotropic within the cone of the solid angle to the Sun subtended by any point at the TOA. Under this assumption, we have

$$I_{\lambda}^r = I_{\lambda}^{Sun} \quad (12)$$

Substitution of TOA specific solar energy intensity  $I_{\lambda}^r$  into Planck expression (2), we get corresponding specific solar entropy intensity at the TOA ( $L_{\lambda}^r$ ) as

$$L_{\lambda}^r = L_{\lambda}^{Sun} \quad (13)$$

#### 4.2 Determination of solar entropy flux received at the TOA

A schematic of the Sun-Earth system is shown in Figure 6. The cone of the solid angle to the Sun subtended by the cross point C of OD and the TOA is formed by its zenith angle  $\theta$  and azimuth angle  $2\pi$ . The incident spectral solar entropy flux ( $J_{\lambda}^r$ ,  $\text{W m}^{-2} \text{K}^{-1} \text{nm}^{-1}$ ) at the TOA can

be readily calculated by integrating the known incident specific solar entropy intensity over the solid angle to the Sun. Details are shown in the following.

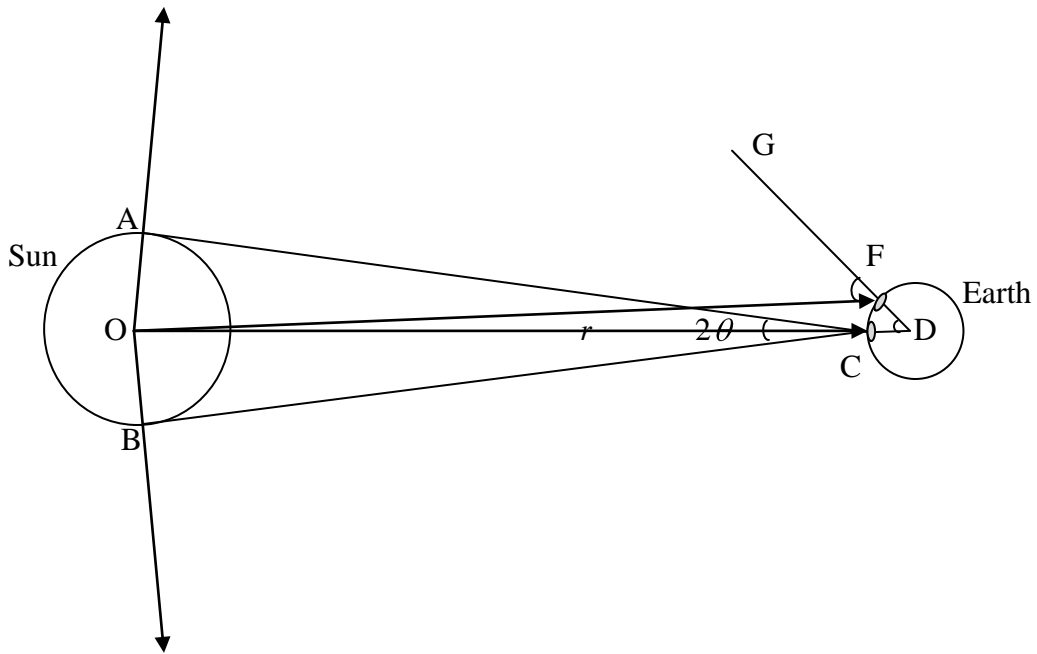


Figure 6. A schematic of the Sun-Earth system. O represents the center of the Sun and D represents the center of the Earth. AC and BC are tangent to the Sun's surface at A and B respectively. C is the cross point of OD and the TOA. F is the cross point of DG and the TOA.  $r$  represents the distance (i.e., 1 AU) between the Sun and the Earth.  $2\theta$  represents the acute angle formed by BC and AC.

Under the assumption I, the incident spectral solar entropy flux ( $J_\lambda^r$ ,  $\text{W m}^{-2} \text{K}^{-1} \text{nm}^{-1}$ ) received at the point C over an infinitesimal TOA area element ( $d\sigma$ ) (i.e., perpendicular to the cone of incident solar beams) can be calculated by integrating the known incident specific solar entropy intensity received at the TOA [ $L_\lambda^r$ , see Eq. (10)] over a hemispheric solid angle, that is,

$$J_\lambda^r(C) = \int_{\Omega_r} L_\lambda^r \cos \theta d\Omega = \int_0^{2\pi} d\varphi \int_0^{\pi/2} L_\lambda^r \sin \theta \cos \theta d\theta = L_\lambda^r \pi \quad (14)$$

$$= \frac{2\pi kC}{\lambda^4} \left\{ \left( 1 + \frac{r_{Sun}^2}{r^2} \frac{\lambda^5 I_\lambda^{Sun}}{2hc^2} \right) \ln \left( 1 + \frac{r_{Sun}^2}{r^2} \frac{\lambda^5 I_\lambda^{Sun}}{2hc^2} \right) - \left( \frac{r_{Sun}^2}{r^2} \frac{\lambda^5 I_\lambda^{Sun}}{2hc^2} \right) \ln \left( \frac{r_{Sun}^2}{r^2} \frac{\lambda^5 I_\lambda^{Sun}}{2hc^2} \right) \right\} \quad (15)$$

Under the assumption II, the specific solar entropy intensity received at the TOA equals that radiated at the Sun's surface and the incident solar radiation is isotropic within the cone of the solid angle to the Sun subtended by any point at the TOA. For a blackbody Sun as assumed in this section, the second half of the assumption II holds as long as the first half of the assumption II holds. Thus, the incident spectral solar entropy flux ( $J_\lambda^r$ ,  $\text{W m}^{-2} \text{K}^{-1} \text{nm}^{-1}$ ) received at the point C over an infinitesimal TOA area element ( $d\sigma$ ) (i.e., perpendicular to the cone of incident solar beams) can be calculated by integrating the known incident specific solar entropy intensity ( $L_\lambda^r = L_\lambda^{Sun}$ ) received at the TOA over the solid angle to the Sun subtended by the point C, that is,

$$J_\lambda^r(C) = \int_{\Omega_r} L_\lambda^r \cos \theta d\Omega = \int_0^{2\pi} d\varphi \int_0^\theta L_\lambda^{Sun} \sin \theta \cos \theta d\theta = L_\lambda^{Sun} \pi [\sin(\theta)]^2 = \frac{r_{Sun}^2}{r^2} J_\lambda^{Sun} \quad (16)$$

where

$$\sin(\theta) = \frac{r_{Sun}}{r} \quad (17)$$

$$J_{\lambda}^{Sun} = L_{\lambda}^{Sun} \pi \quad (18)$$

Note that the solid angle in Eq. (16) is dependent on the solar radiation traveling distance  $r$ .

Now, we know the incident spectral solar entropy flux ( $J_{\lambda}^r$ ,  $\text{W m}^{-2} \text{K}^{-1} \text{nm}^{-1}$ ) received at the point C over an infinitesimal TOA area element ( $d\sigma$ ) (i.e., perpendicular to the cone of incident solar beams) under the two different assumptions. Based on this, the incident spectral solar entropy flux ( $J_{\lambda}^r$ ) received at any given point (F) over an infinitesimal TOA area element ( $d\sigma$ ) can be obtained by

$$J_{\lambda}^r(F) = J_{\lambda}^r(C) \cos \beta = J_{\lambda}^r(C) \cos(\alpha + \gamma) \quad (19)$$

where  $\alpha$ ,  $\beta$ , and  $\gamma$  represent the angles formed respectively by CD and DF, by OF and FG, and by FO and OC.

Thus, the total incident entropy per unit wavelength ( $S_{\lambda}^r$ ,  $\text{W K}^{-1} \text{nm}^{-1}$ ) received at the TOA can be calculated by integrating  $J_{\lambda}^r(F)$  over the area of the TOA hemisphere facing the Sun, i.e.,

$$S_{\lambda}^r = \int_{\text{TOA}} J_{\lambda}^r(F) d\sigma = \int_0^{2\pi} d\varphi \int_0^{\pi/2} J_{\lambda}^r(C) \cos(\alpha + \gamma) r_{\text{Earth}}^2 \sin \alpha d\alpha \quad (20)$$

$$= 2\pi r_{\text{Earth}}^2 J_{\lambda}^r(C) \int_0^{\pi/2} \cos(\alpha + \gamma) \sin \alpha d\alpha \quad (21)$$

$$\approx 2\pi r_{\text{Earth}}^2 J_{\lambda}^r(C) \int_0^{\pi/2} \cos \alpha \sin \alpha d\alpha \quad (22)$$

$$= \pi r_{\text{Earth}}^2 J_{\lambda}^r(C) \quad (23)$$

where the approximate equality from Eq. (21) to Eq. (22) is based on the fact that OF is approximately equal to OD and the fact that  $\frac{\sin[\pi - (\alpha + \gamma)]}{\text{OD}} = \frac{\sin \alpha}{\text{OF}}$ .

The globally averaged incident spectral solar entropy flux received at the TOA can be derived as [based on Eq. (23)]

$$\bar{J}_\lambda^r = \frac{S_\lambda^r}{4\pi r_{Earth}^2} = \frac{J_\lambda^r(C)}{4} \quad (24)$$

Equation (24) reveals that the globally averaged incident spectral solar entropy flux received at the TOA is equal to one quarter of the incident spectral solar entropy flux received over an infinitesimal TOA area element perpendicular to the cone of incident solar beams. Likewise, the globally averaged incident spectral solar energy flux received at the TOA should be equal to one quarter of the incident spectral solar energy flux received over an infinitesimal TOA area element perpendicular to the cone of incident solar beams.

Integration of Eq. (24) over all wavelengths leads to the globally averaged incident solar entropy flux received at the TOA as

$$\bar{J}^r = \int_0^\infty \bar{J}_\lambda^r d\lambda = \frac{1}{4} \int_0^\infty J_\lambda^r(C) d\lambda \quad (25)$$

Substitution of Eq. (16) into Eq. (25) leads to the globally averaged incident solar entropy flux received at the TOA for a blackbody Sun under the assumption II as

$$\bar{J}^r = \frac{r_{Sun}^2}{4r^2} \int_0^\infty J_\lambda^{Sun} d\lambda = \frac{1}{4} \left( \frac{r_{Sun}^2}{r^2} J^{Sun} \right) = \frac{1}{4} \left[ \frac{r_{Sun}^2}{r^2} \left( \frac{4}{3} \sigma T_{Sun}^3 \right) \right] \quad (26)$$

#### 4.3. Discussion on the conventional expression (5)

If the globally averaged cosine of solar zenith angle is assumed as  $\cos\theta_0 = 0.25$  and solar solid angle equals  $\Omega_0 = 6.77 \times 10^{-5}$  sr to the planet as in Stephens and O'Brien (1993), the conventional expression (5) can be re-written as

$$J = \frac{4}{3} \sigma T_{Sun}^3 \cos \theta_0 \frac{\Omega_0}{\pi} \quad (5)$$

$$= \left( \frac{4}{3} \sigma T_{Sun}^3 \right) \frac{1}{4\pi} \left( \int_0^{2\pi} d\varphi \int_0^\theta \sin \theta d\theta \right) \quad (27)$$

$$\approx \left( \frac{4}{3} \sigma T_{Sun}^3 \right) \frac{1}{4\pi} \left( \int_0^{2\pi} d\varphi \int_0^\theta \sin \theta \cos \theta d\theta \right) \quad (28)$$

$$= \left( \frac{4}{3} \sigma T_{Sun}^3 \right) \frac{1}{4\pi} \pi [\sin(\theta)]^2 \quad (29)$$

$$= \frac{1}{4} \left[ \frac{r_{Sun}^2}{r^2} \left( \frac{4}{3} \sigma T_{Sun}^3 \right) \right] \quad (30)$$

where the solar solid angle  $\Omega_0 = 6.77 \times 10^{-5}$  sr to the planet in Eq. (27) has been written back as

$$\Omega_0 = \int_0^{2\pi} d\varphi \int_0^\theta \sin \theta d\theta \quad (31)$$

and the approximate equality from Eq. (27) to Eq. (28) is based on the fact that the solar zenith angle  $\theta$  is small (or  $\theta \ll 1$ ) so that  $\cos \theta \approx 1$ .

Equations (26) and (30) reveals that the conventional expression (5) given by Stephens and O'Brien (1993) represents essentially the globally averaged incident solar entropy flux received at the TOA for a blackbody Sun under the assumption II with the globally averaged cosine of solar zenith angle equals  $\cos \theta_0 = 0.25$  and solar solid angle equals  $\Omega_0 = 6.77 \times 10^{-5}$  sr. This equality explains why the estimated globally averaged Earth's incident solar entropy flux from the conventional expression (5) is about the same as that estimated under the assumption II for the blackbody Sun as discussed in the last section.

## **5. Sensitivity of the Earth's incident solar radiation entropy flux to TOA SSI variability**

To further explore the sensitivity of the Earth's incident solar radiation entropy flux to TOA SSI variability, this section uses the mean SIM-based TOA SSI distribution within [200 nm, 2400 nm] wavelengths and construct two additional TOA SSI scenarios in the corresponding wavelengths. The two constructed TOA SSI scenarios have the same overall solar irradiance within the wavelengths from 200nm to 2400 nm as the mean SIM-based TOA SSI. Scenario I represents the TOA SSI of a blackbody Sun. Scenario II represents the TOA SSI of a non-blackbody Sun, with the Sun's brightness temperature represented by a combination of two half-period sinusoidal curves over [200 nm, 800 nm] wavelengths and over [801 nm, 2400 nm] wavelengths. The incident spectral solar radiation entropy fluxes over the wavelengths from 200 nm to 2400 nm are examined using Planck expression for the three cases. Integration of the incident spectral solar radiation entropy flux over the wavelengths from 200 nm to 2400 nm further leads to the overall incident solar radiation entropy flux within [200 nm, 2400 nm] wavelengths. The magnitudes and spectral distributions of the resulting Earth's incident solar radiation entropy fluxes within [200 nm, 2400 nm] wavelengths for the three cases are then compared. For simplification, the sensitivity study shown in this section is conducted under the assumption I. Similar study can be conducted straightforward under the assumption II.

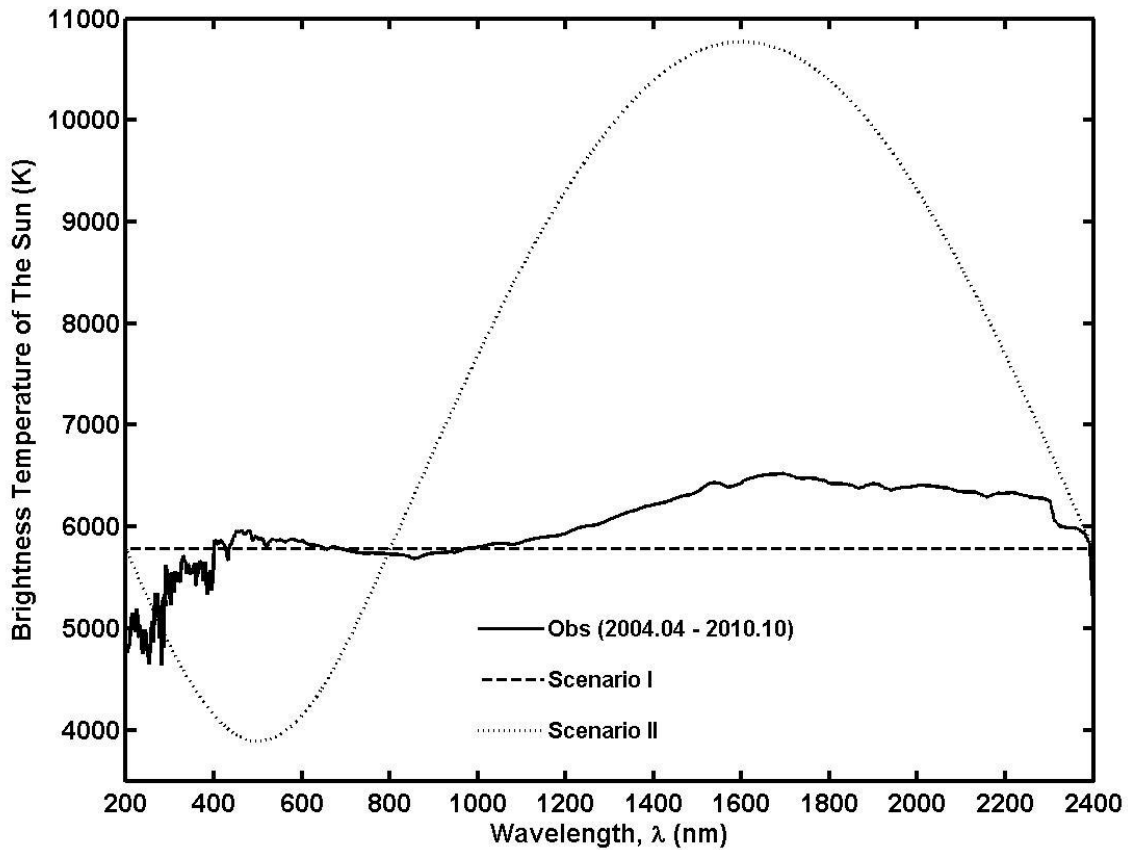


Figure 7. The Sun's brightness temperature as a function of wavelength within [200 nm, 2400 nm]. Black solid line: brightness temperature corresponding to the mean SIM-based SSI from 04/2004 to 10/2010. Black dashed or dotted lines: brightness temperatures corresponding to the two constructed TOA SSI scenarios with the same overall solar irradiance within the wavelengths from 200nm to 2400 nm as the mean SIM-based TOA SSI.

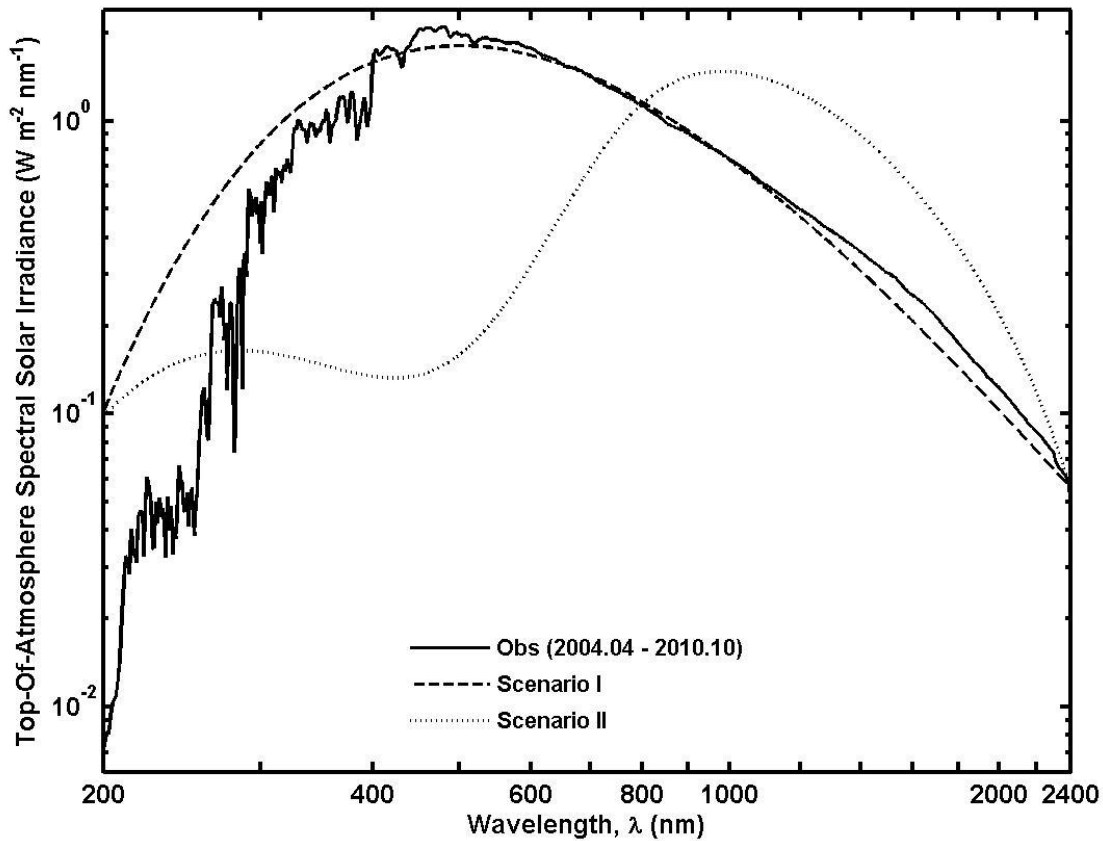


Figure 8. The Earth's incident spectral solar radiation energy flux for the three cases as shown in Figure 7.

Figure 7 shows the Sun's brightness temperature as a function of wavelength within [200 nm, 2400 nm] corresponding to the mean SIM-based TOA SSI distribution (black solid line) and the two constructed TOA SSI scenarios (black dashed or dotted lines) as described above. The distributions of their corresponding Earth's incident spectral solar radiation energy flux are shown in Figure 8.

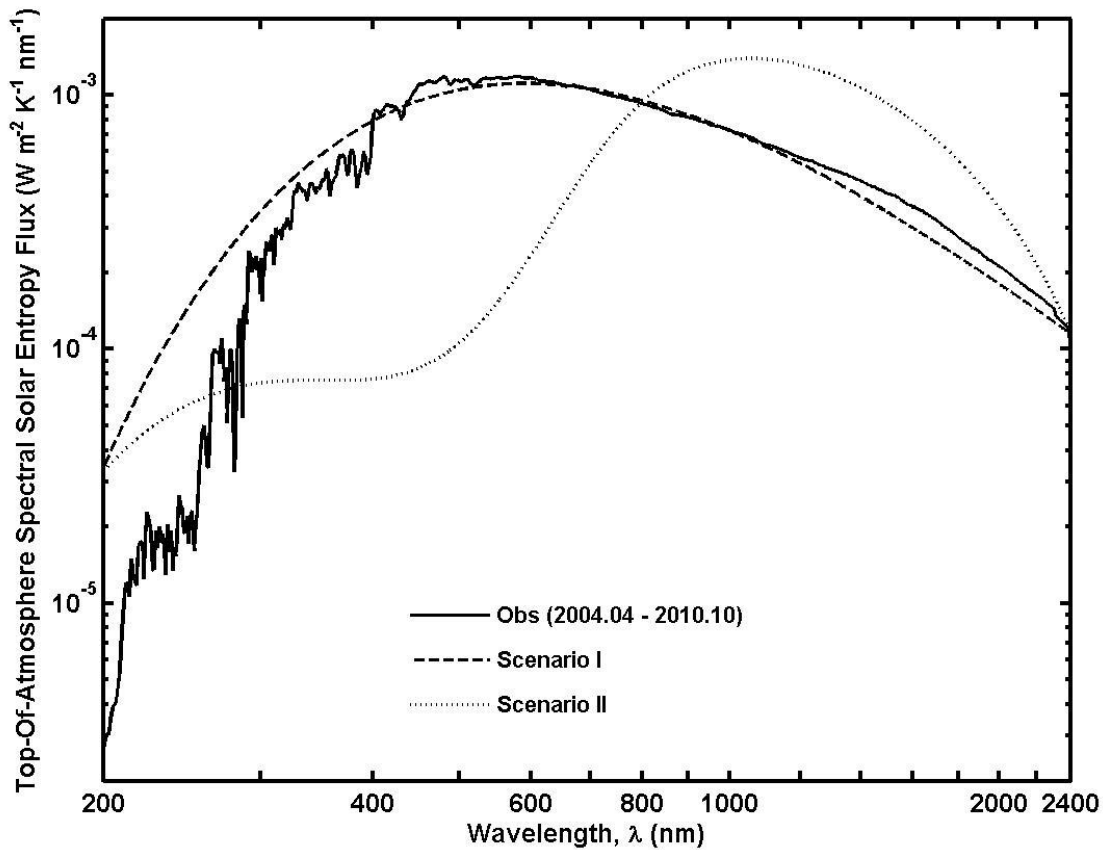


Figure 9. The Earth's incident spectral solar radiation entropy flux for the three cases as shown in Figure 7 or Figure 8.

Figure 9 shows the Earth's incident spectral solar radiation entropy flux for the three cases. As can be seen, the Earth's incident solar radiation entropy fluxes present similar patterns to their corresponding incident solar radiation energy fluxes as shown in Figure 8. Compared with scenario I (a blackbody Sun), the Earth's incident solar radiation entropy flux from the SIM-based TOA SSI shows relatively low entropy flux at ultraviolet (< 400 nm) wavelengths, relatively high entropy flux at visible (400 nm to 700 nm) and the near-infrared (1000 nm to

2400 nm) wavelengths, and slightly relatively low entropy flux at the near-infrared (700 nm to 1000 nm) wavelengths. On the other hand, the Earth's incident solar radiation entropy flux from scenario II (a non-blackbody Sun) in general is much lower at the wavelengths less than 800 nm and much higher at the wavelengths larger than 800 nm than those from the other two cases, except for the wavelengths less than 280 nm where the Earth's incident solar radiation entropy flux from the SIM-based TOA SSI is much lower than that from the others.

By further integrating the Earth's incident spectral solar radiation entropy flux over the wavelength range of [200nm, 2400 nm], we obtain the estimates of the overall Earth's incident solar radiation entropy flux within [200 nm, 2400 nm] wavelengths for the three cases. They are  $1.13 \text{ W m}^{-2} \text{ K}^{-1}$  for the mean SIM-based TOA SSI,  $1.09 \text{ W m}^{-2} \text{ K}^{-1}$  for scenario I, and  $1.40 \text{ W m}^{-2} \text{ K}^{-1}$  for scenario II. In other words, the overall incident solar radiation entropy flux within [200 nm, 2400 nm] from the mean SIM-based TOA SSI (or scenario II) is  $0.04 \text{ W m}^{-2} \text{ K}^{-1}$  [or  $0.31 \text{ W m}^{-2} \text{ K}^{-1}$ ] larger than that from scenario I. Notice that, the difference of  $0.31 \text{ W m}^{-2} \text{ K}^{-1}$  is more than the typical value of the entropy production rate associated with the atmospheric latent heat process  $0.30 \text{ W m}^{-2} \text{ K}^{-1}$  according to Peixoto et al. (1991).

## 6. Summary

The magnitude and spectral distribution of the Earth's incident solar radiation entropy flux are examined using the TOA SSI observations from the SORCE SIM instrument. The examination is conducted under two common assumptions regarding the distribution of incident solar radiation at the TOA: assumption I. isotropic hemispheric solar radiation, assumption II. the specific solar energy intensity received at the TOA is the same as that radiated at the Sun's surface and incident solar radiation is isotropic within the cone of the solid angle to the Sun subtended by

any point at the TOA. The Earth's incident solar radiation entropy flux estimated by using the SIM-based TOA SSI and Planck expression of specific entropy intensity under the two assumptions is examined and further compared with that estimated by using a conventional expression based on the Sun's brightness temperature under the assumption of a blackbody Sun. The potential cause of the large difference exhibited among the estimates is revealed. Furthermore, sensitivity experiments are performed to investigate the significance of the impact of TOA SSI variability on estimation of the Earth's incident solar radiation entropy flux.

The Earth's incident solar radiation entropy flux estimated using the mean SIM-based TOA SSI observations and Planck expression of specific entropy intensity under the assumption I shows 4 times larger in magnitude than that under the assumption II. The latter is about the same as that estimated using the conventional expression based on the Sun's brightness temperature under the assumption of a blackbody Sun. It is worth emphasizing that the difference ( $0.23 \text{ W m}^{-2} \text{ K}^{-1}$ ) between the estimate under the assumption I and the estimate under the assumption II (or the estimate from the conventional approach) represents about 77% of the typical entropy production rate associated with the atmospheric latent heat process (Peixoto et al., 1991). It is shown that under the assumption I the decrease of specific solar entropy intensity with radiation traveling distance, unlike the decrease of specific solar energy intensity with radiation traveling distance, is wavelength dependent. This is different from the case under the assumption II where specific solar energy and entropy intensities are both independent on radiation traveling distance. That explains why the estimates of the Earth's incident solar radiation entropy flux under the two different assumptions show a significant difference in magnitude.

In addition, it is theoretically shown that the conventional expression essentially represents the globally averaged incident solar entropy flux received at the TOA derived for a blackbody Sun under the assumption II with the globally averaged cosine of solar zenith angle equals  $\cos\theta_0 = 0.25$  and solar solid angle equals  $\Omega_0 = 6.77 \times 10^{-5}$  sr . The theoretical formulation clearly explains why the estimated globally averaged Earth's incident solar entropy flux from the conventional approach is about the same as that estimated for the blackbody Sun under the assumption II as shown in Section 3.

It is worth mentioning that in reality the Earth's incident solar radiation probably does not behave as the assumption I of isotropic hemistropic solar radiation that requires the space is full of scattering particles. Neither does it completely as the assumption II with the necessary conditions that the space between the Earth and the Sun is empty, nothing happens to the traveling solar photons in space (i.e., no scattering, absorption, emission) ,and the Sun behaves as a blackbody (i.e., homogeneously emitting isotropic photons). The real situation likely operates between the conditions underlying the two common assumptions, probably relatively closer to that under the assumption II. The formulation presented here may be useful to future exploration along this line.

Moreover, our sensitivity experiments show that even for the same overall TOA solar irradiance, the Earth's incident solar radiation entropy flux can change significantly in both magnitude and spectral distribution with the change of TOA SSI distribution. The difference in magnitude of the resulting Earth's incident solar radiation entropy flux between some cases could be larger than the typical value of the entropy production rate associated with the atmospheric latent heat process. These results together highlight the importance and necessity of

knowing the non-blackbody TOA SSI variability in calculation of the Earth's incident solar radiation entropy flux, and hence the Earth's radiation entropy budget and climate.

It is noted that although the significance of the impact of TOA SSI variability on the entropy production inside the Earth's climate system is beyond the scope of this work, a substantial impact is possible and expected critical to determining the Earth system's thermodynamic quantities such as energy transport, temperature or humidity profiles, cloud processes. This is somewhat evident by the fact that both magnitude and spectral distribution of the Earth's incident solar radiation entropy flux could change significantly with TOA SSI variability. Considering that the Earth's incident solar radiation at different wavelengths reaches and warms different atmospheric layers, such a significant change on the Earth's incident solar radiation entropy flux could possibly lead to a substantial impact on the entropy production produced at different Earth's atmospheric layers. Besides, the impact of TOA SSI variability on the entropy production of the Earth's climate system comes not only from incident solar radiation but also from reflected solar radiation or even emitted terrestrial radiation, because the thermal structure of the Earth's climate system could vary significantly with the changing TOA SSI (e.g., Cahanlan et al. 2010; Haigh et al., 2010).

It is also noted that this study is just a beginning to explore the importance of spectral solar irradiance and its variation in determining the Earth's radiation entropy and climate. Much remains to be learned. For example, the relative agreement between the overall magnitudes of the Earth's incident solar radiation entropy flux by applying the mean SIM-based TOA SSI or the TOA SSI from a corresponding blackbody Sun (i.e., with the same amount of TOA TSI) into Planck expression holds only true for the cases investigated here. Large discrepancy cannot be

ruled out for other cases. Also, little has been known on the potential influences of TOA SSI variability on the entropy production produced by the processes occurring inside the Earth's climate system, such as clouds and precipitation. Research along these lines is highly recommended.

**Acknowledgment.** This work is supported by the ESM (Earth System Modeling) through the FASTER project ([www.bnl.gov/esm](http://www.bnl.gov/esm)), and ASR (Atmospheric Science Research) programs of the U. S. Department of Energy. We are grateful to Fabian Gans at Max-Planck-Institute for insightful comments and for providing us a detailed clarification on the comment that solar solid angle may change with radiation traveling distance, which leads to our study related to the assumption II. We are also grateful to the anonymous reviewer for positive and insightful comments, and to Stephen E. Schwartz at BNL for valuable discussions.

## References

- Cahanlan, R. F., Wen, G. Y., Harder, J. W., and Pilewskie, P.: Temperature responses to spectral solar variability on decadal time scales. *Geophys. Res. Lett.*, 37, L07705, doi:10.1029/2009GL041898, 2010.
- Gray, L. J., Beer, J., Geller, M., Haigh, J. D., Lockwood, M., Matthes, K., Cubasch, U., Fleitmann, D., Harrison, G., Hood, L., Luterbacher, J., Meehl, G. A., Shindell, D., Van Geel, B., and White, W.: Solar influences on climate, *Rev. Geophys.*, 48, RG4001, doi:10.1029/2009RG000282, 2010.
- Haigh, J. D., Winning, A. R., Toumi, R., and Harder, J. W.: An influence of spectral solar variations on radiative forcing of climate, *Nature*, 467, 696- 699, doi:10.1038/nature09426, 2010.
- Harder, J., Lawrence, G., Fontenla, J., Rottman, G., and Woods, T.: The spectral irradiance monitor: Scientific requirements, instrument design, and operation modes, *Sol. Phys.*, 230, 141-167, 2005.
- Harder, J. W., Fontenla, J. M., Pilewskie, P., Richard, E. C. & Woods, T. N.: Trends in spectral solar irradiance variability in the visible and infrared. *Geophys. Res. Lett.*, 36, L07801, doi:10.1029/2008GL036797, 2009.
- Jupp, T. E., Cox, P. M.: MEP and planetary climates: insights from a two-box climate model containing atmospheric dynamics, *Phil. Trans. R. Soc. B*, 365, 1355-1365, doi:10.1098/rstb.2009.0297, 2010.

- Kleidon, A., Malhi, Y., and Cox, P. M.: Maximum entropy production in environmental and ecological systems, *Philos. Trans. R. Soc. B*, 365, 1297–1302, doi:10.1098/rstb.2010.0018, 2010.
- Lean, J.: Evolution of the Sun's spectral irradiance since the Maunder minimum, *Geophys. Res. Lett.*, 27, 2425-2428, 2000.
- Liu, Y., Liu, C., and Wang, D.: Understanding atmospheric behaviour in terms of entropy: a review of applications of the second law of thermodynamics to meteorology, *Entropy*, 13, 211-240; doi:10.3390/e13010211, 2011.
- Lorenz, R.: The two-box model of climate: limitations and applications to planetary habitability and maximum entropy production studies, *Phil. Trans. R. Soc. B*, 365, 1349-1354, doi:10.1098/rstb.2009.0312, 2010.
- Lucarini, V., Fraedrich, K., and Lunkeit, F.: Thermodynamics of climate change: Generalized sensitivities, *Atmos. Chem. Phys. Discuss.*, 10, 3699–3715, 2010.
- Ozawa, H., Shimokawa, S., Sakuma, H.: Thermodynamics of fluid turbulence: A unified approach to the maximum transport properties, *Phys. Rev. E*, 64, 026303, doi:10.1103/PhysRevE.64.026303, 2001.
- Pauluis, O., and Held, I. M.: Entropy budget of an atmosphere in radiative-convective equilibrium. Part I: Maximum work and frictional dissipation, *J. Atmos. Sci.*, 59, 125–139, 2002a.
- Pauluis, O., and Held, I. M.: Entropy budget of an atmosphere in radiative-convective equilibrium. Part II: Latent heat transport and moist processes, *J. Atmos. Sci.*, 59, 140–149, 2002b.

- Paltridge, G. W., Farquhar, G. D., and Cuntz, M.: Maximum entropy production, cloud feedback, and climate change. *Geophys. Res. Lett.*, 34, 1–6, L14708, doi:10.1029/2007GL029925, 2007.
- Peixoto, J. P., Oort, A. H., De Almeida, M., and Tomé, A.: Entropy budget of the atmosphere, *J. Geophys. Res.*, 96, 10,981–10,988, doi:10.1029/91JD00721, 1991.
- Planck, M.: *The Theory of Heat Radiation*, 224 pp., 1913. (English translation by Morton Mausius (1914), Dover Publications, New York, 1959).
- Pujol, T., and Fort, J.: States of maximum entropy production in a one-dimensional vertical model with convective adjustment. *Tellus*, 54A, 363–369, 2002.
- Rottman, G., Harder, J., Fontenla, J., Woods, T. N., White, O. R., and Lawrence, G.: The Spectral Irradiance Monitor (SIM): Early observations, *Sol. Phys.*, 230, 205-224, 2005.
- Stephens, G. L., and O'Brien, D. M.: Entropy and climate, I, ERBE observations of the entropy production, *Q. J. R. Meteorol. Soc.*, 119, 121–152, 1993.
- Wang, B, Nakajima, T, Shi, G.: Cloud and Water Vapor Feedbacks in a Vertical Energy-Balance Model with Maximum Entropy Production, *J. Clim.*, 21, 6689-6697, doi:10.1175/2008JCLI2349.1., 2008.
- Wu, W., and Liu Y.: Radiation entropy flux and entropy production of the Earth system. *Rev. Geophys.*, 48, RG2003, doi:10.1029/2008RG000275, 2010a.
- Wu, W., and Liu Y.: A new one-dimensional radiative equilibrium model for investigating atmospheric radiation entropy flux, *Philos. Trans. R. Soc. B*, 365, 1367–1376, doi:10.1098/rstb.2009.0301, 2010b.

## Figure Captions

Figure 1. Black solid line represents the mean SIM-based TOA SSI distribution based on the data collected from 04/2004 to 10/2010. Black dashed line represents the TOA SSI distribution corresponding to a blackbody Sun with brightness temperature 5770 K.

Figure 2. The Earth's incident spectral solar radiation entropy flux corresponding to the TOA SSIs as shown in Figure 1. Black solid and dashed lines are calculated under the assumption I of isotropic hemispheric solar radiation. Gray solid and dashed lines are calculated under the assumption II that the specific solar energy intensity received at the TOA is the same as that radiated at the Sun's surface and incident solar radiation is isotropic within the cone of the solid angle to the Sun subtended by any point at the TOA.

Figure 3. Specific solar energy intensity at the Sun's surface (black solid line) and that at 1 AU scaled by  $\{\max(I_{\lambda}^{Sun})/[2\max(I_{\lambda}^{1AU})]\}$  (black dashed line), for a blackbody Sun with brightness temperature 5770 K under the assumption I of isotropic hemispheric solar radiation.

Figure 4. Specific solar entropy intensity at the Sun's surface (black solid line) and that at 1 AU scaled by  $\{\max(L_{\lambda}^{Sun})/[2\max(L_{\lambda}^{1AU})]\}$  (black dashed line), for a blackbody Sun with brightness temperature 5770 K under the assumption I of isotropic hemispheric solar radiation.

Figure 5. Black solid line: the ratio of specific solar energy intensity at the Sun's surface and that at 1 AU, for a blackbody Sun with brightness temperature 5770 K under the assumption I of isotropic hemispheric solar radiation. Black dashed line: the ratio of specific solar entropy intensity at the Sun's surface and that at 1 AU for the same blackbody Sun under the assumption I of isotropic hemispheric solar radiation.

Figure 6. A schematic of the Sun-Earth system. O represents the center of the Sun and D represents the center of the Earth. AC and BC are tangent to the Sun's surface at A and B respectively. C is the cross point of OD and the TOA. F is the cross point of DG and the TOA.  $r$  represents the distance (i.e., 1 AU) between the Sun and the Earth.  $2\theta$  represents the acute angle formed by BC and AC.

Figure 7. The Sun's brightness temperature as a function of wavelength within [200 nm, 2400 nm]. Black solid line: brightness temperature corresponding to the mean SIM-based SSI from 04/2004 to 10/2010. Black dashed or dotted lines: brightness temperatures corresponding to the two constructed TOA SSI scenarios with the same overall solar irradiance within the wavelengths from 200nm to 2400 nm as the mean SIM-based TOA SSI.

Figure 8. The Earth's incident spectral solar radiation energy flux for the three cases as shown in Figure 7.

Figure 9. The Earth's incident spectral solar radiation entropy flux for the three cases as shown in Figure 7 or Figure 8.

Figure 1

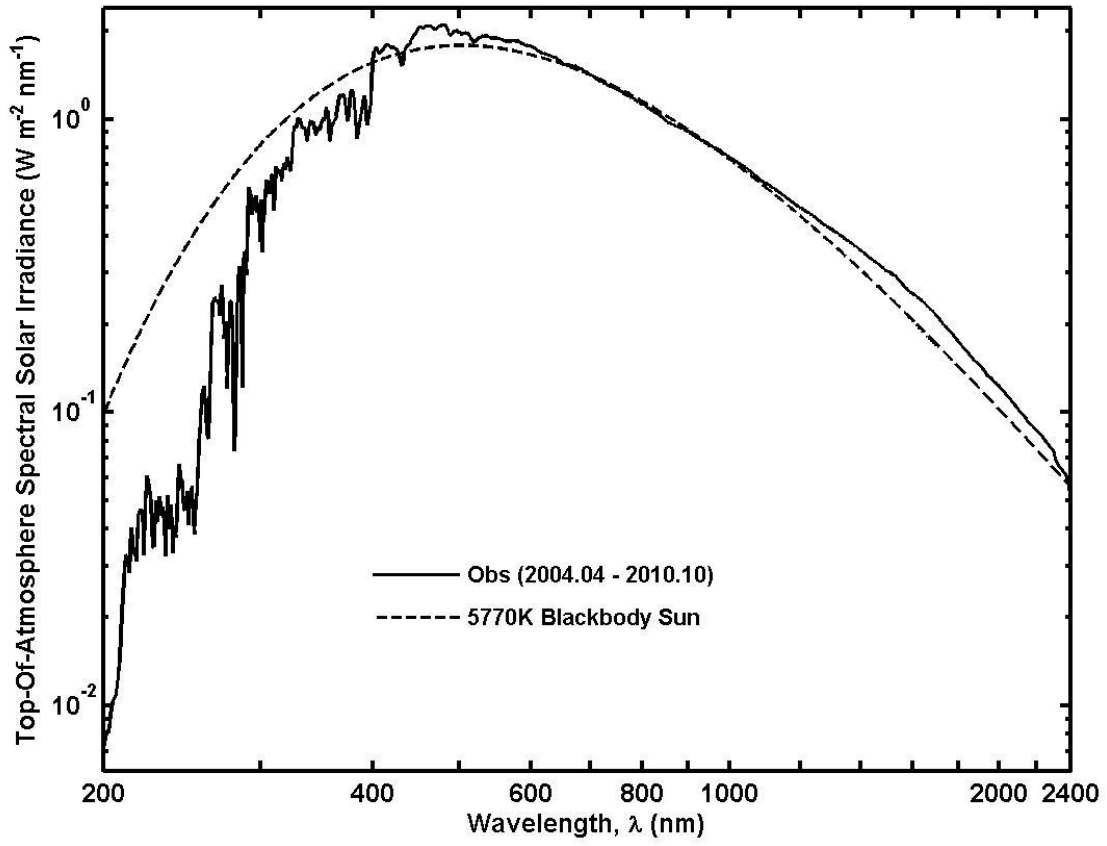


Figure 2

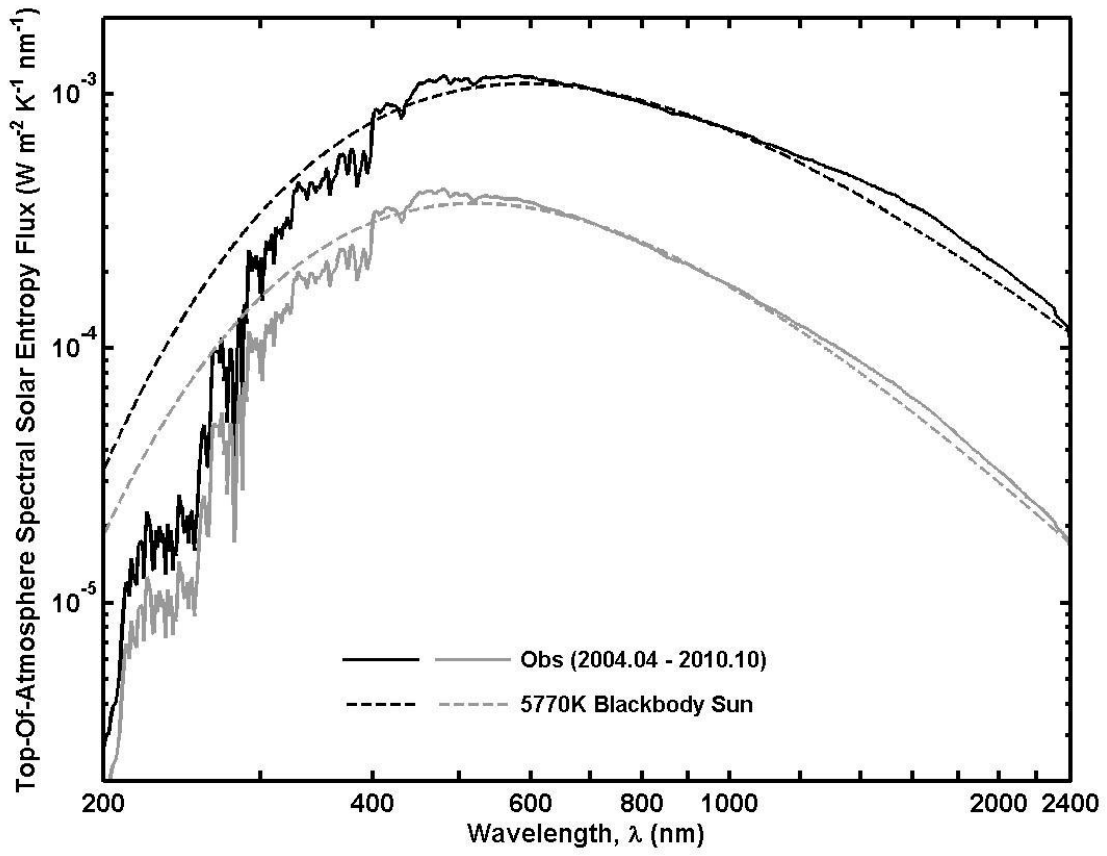


Figure 3

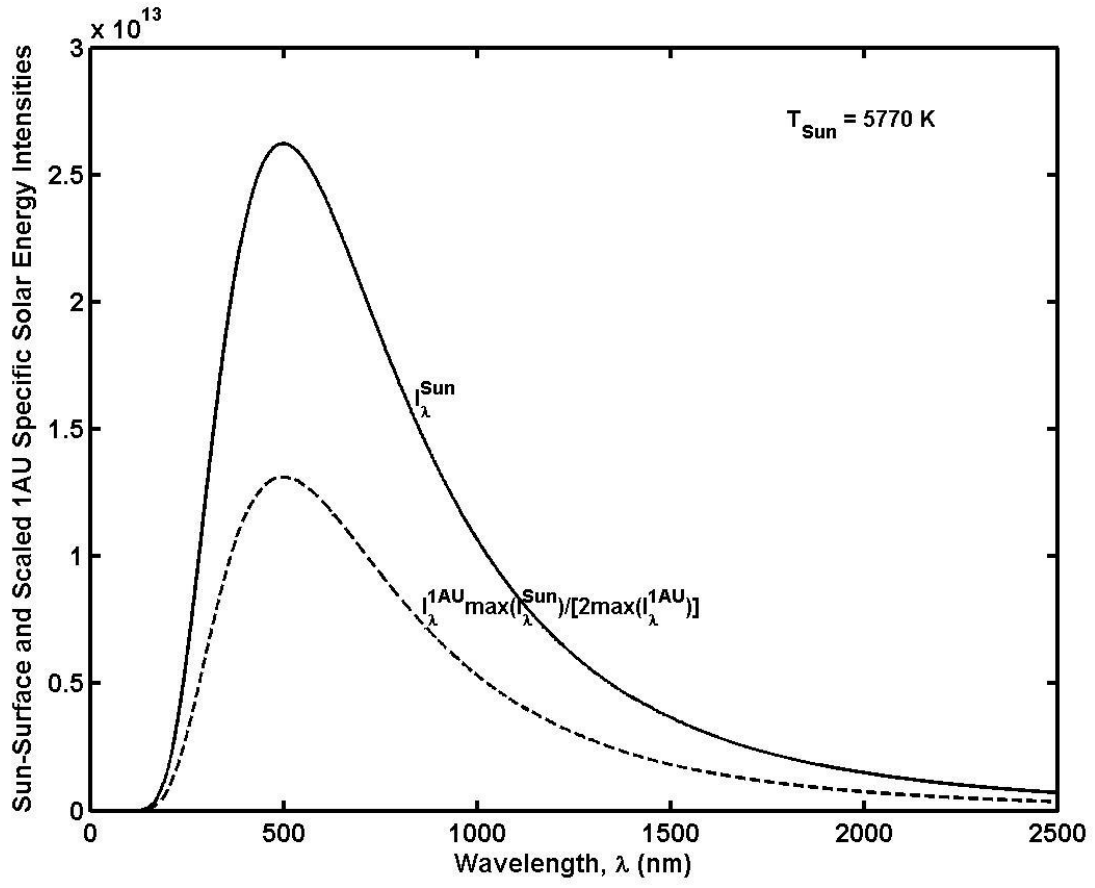


Figure 4

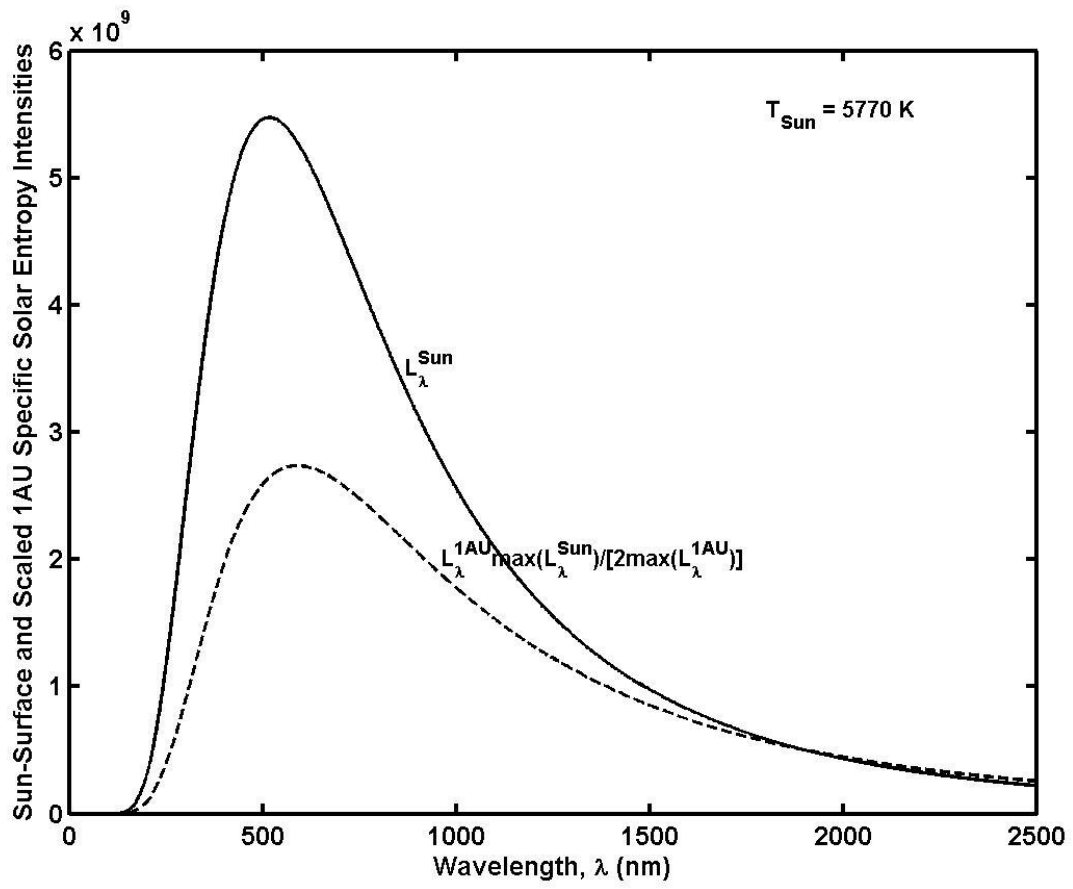


Figure 5

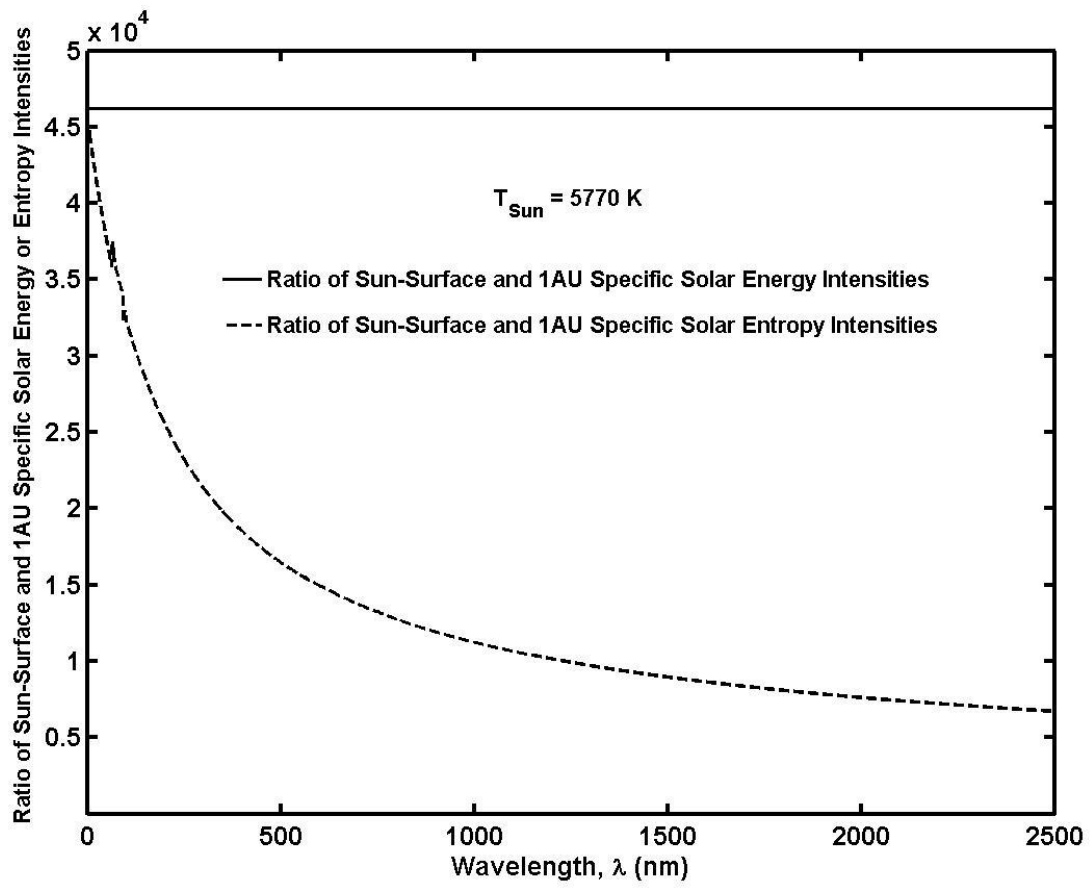


Figure 6

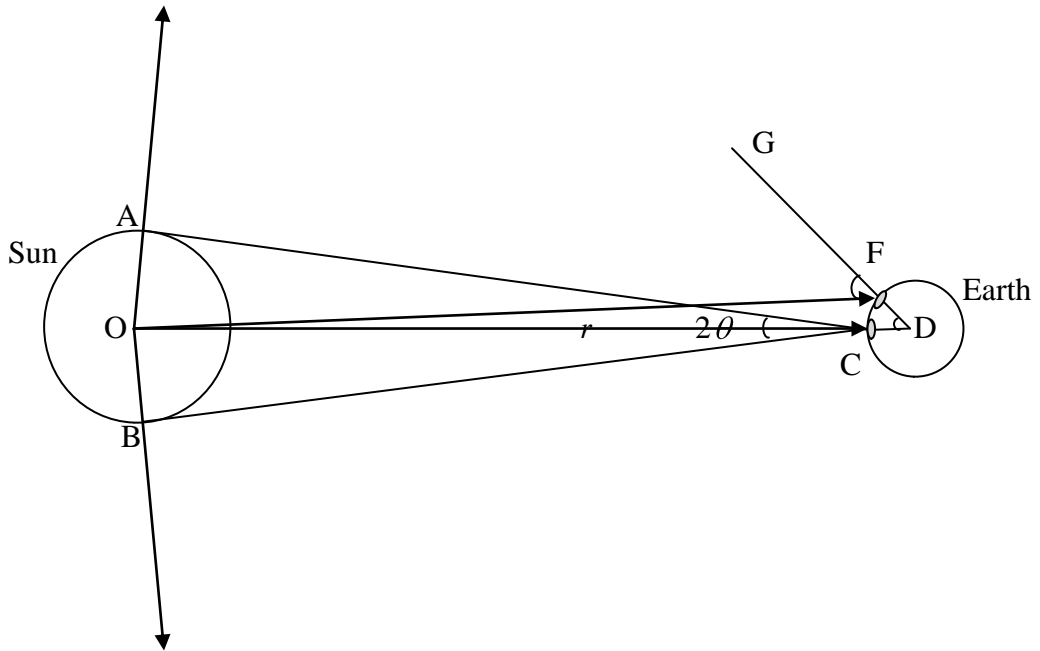


Figure 7

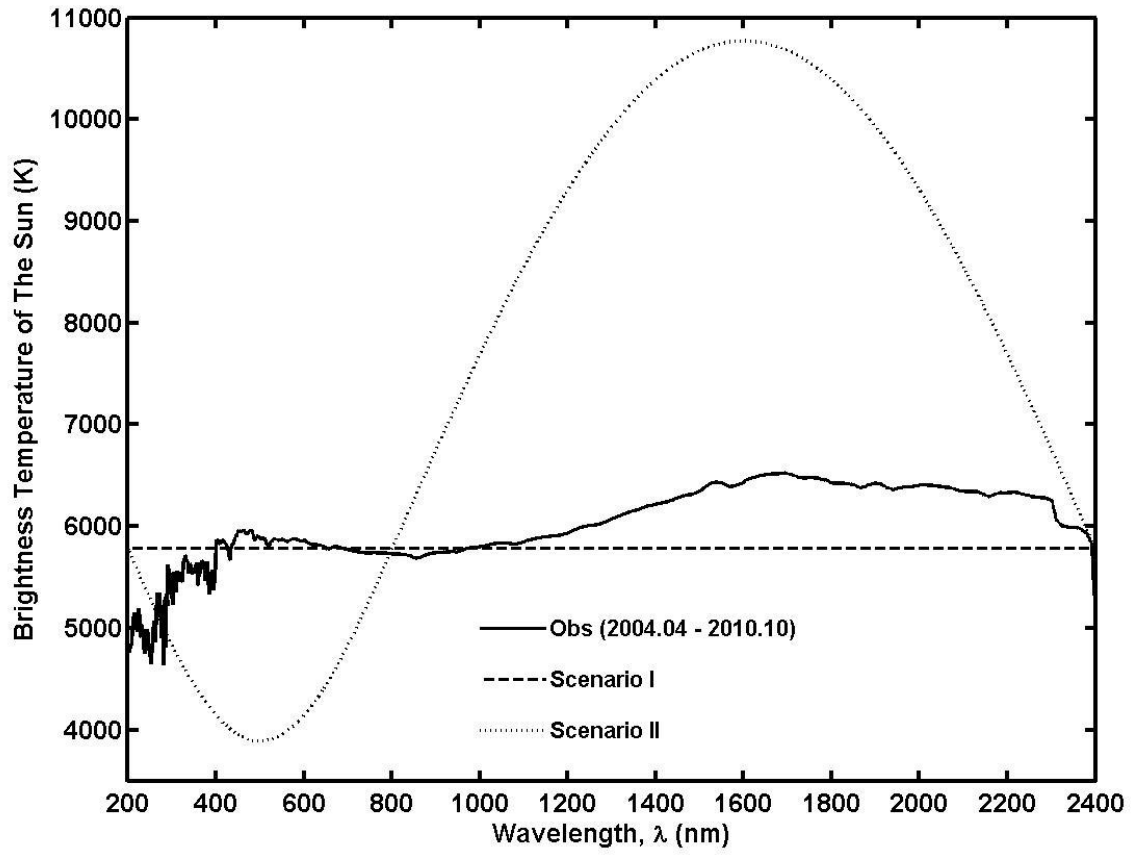


Figure 8

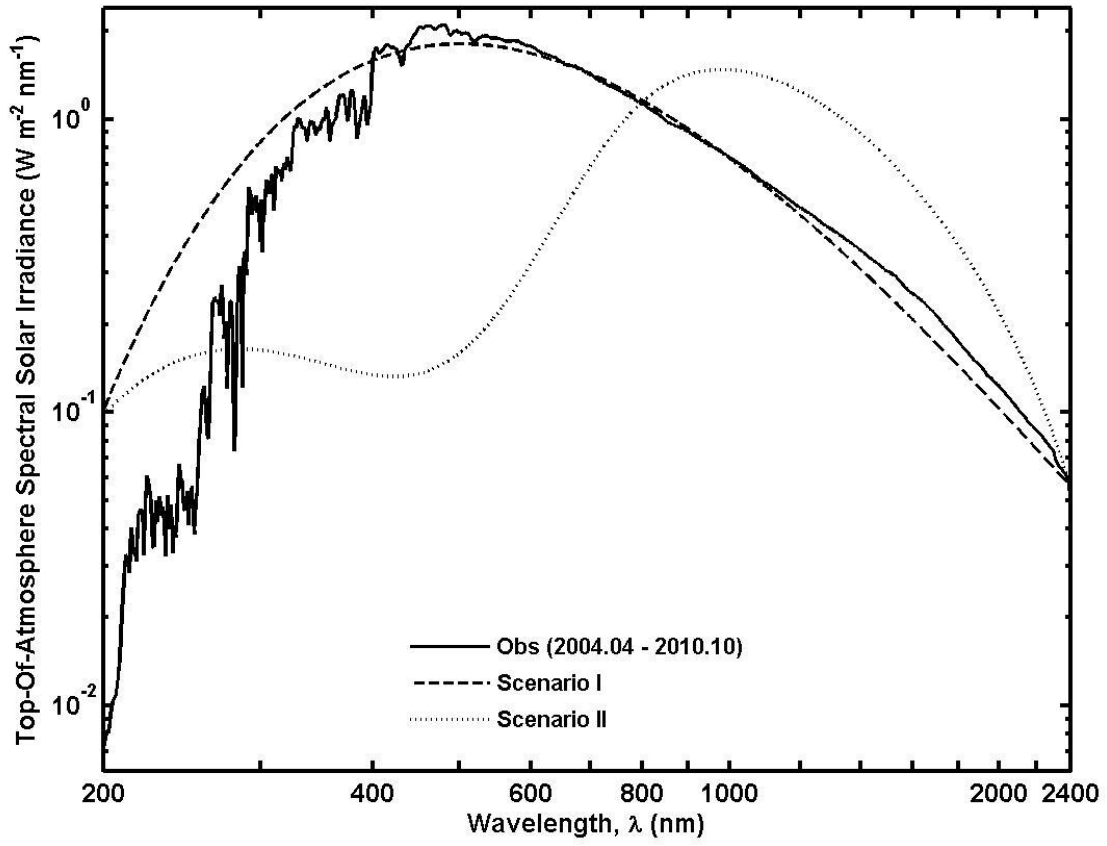


Figure 9

